ACS OMEGA

Open Access

http://pubs.acs.org/journal/acsodf

Article

5-Fluorouracil- and Sesamol-Loaded Transliposomal Gel for Skin Cancer: *In Vitro, Ex Vivo*, and Dermatokinetic Evaluation

Samreen Jahan, Niha Sultana, Asad Ali, Nasr A. Emad, Perwez Alam, Mohd. Mujeeb, Mohd. Aqil,* and Asgar Ali*

Cite This: *ACS Omega* 2025, 10, 6857−6875

Read Online

ACCESS | Metrics & More | Article Recommendations

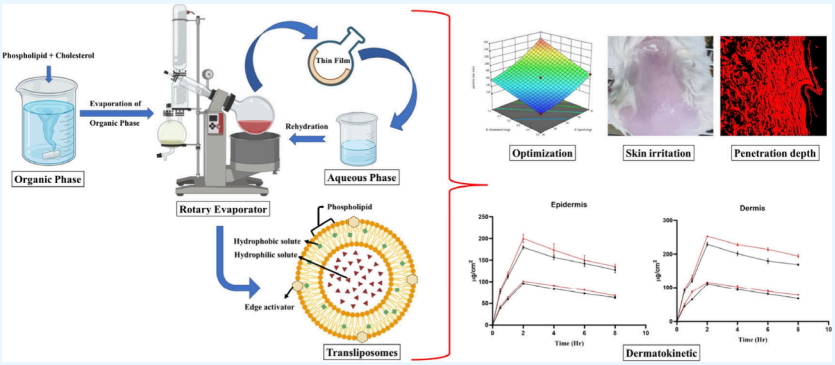

ABSTRACT: This study explores a novel approach to managing skin conditions through a combination therapy utilizing a phospholipid-enriched edge activator-based nanoformulation. 5-Fluorouracil (5-FU)- and sesamol (SES)-loaded transliposomes (FS-TL) were developed using a thin film hydration method and optimized using Box-Behnken Design. FS-TL characterization indicated a vesicle size of 165.6 ± 1.1 nm, polydispersity index of 0.28 ± 0.01, and a zeta potential of −33.17 ± 0.9 mV, and the percent entrapment efficiencies for 5-FU and SES were found to be 63.16 ± 1.07% and 75.60 ± 3.68%, respectively. The drug loading percents for 5-FU and SES were found to be 5.87 ± 0.099% and 7.03 ± 0.34%, respectively. The morphological studies exhibit the distinctive spherical shape of the nanoformulation. The *in vitro* drug release demonstrated sustained release with 82.52 ± 1.2% and 86.28 ± 1.3% releases for 5-FU and SES, respectively. The *ex vivo* skin permeation exhibited 81.04 ± 2.1% and 78.03 ± 1.7% for 5-FU and SES. Confocal laser microscopy scanning (CLSM) revealed a deeper formulation penetration (30.0 μm) of excised mice skin membranes than for a standard rhodamine solution (10.0 μm). The dermatokinetic investigation revealed that FS-TL gel has significantly higher concentrations of 5-FU and SES ($p < 0.001$). The efficacy of FS-TL ($p < 0.05$) in eradicating the A431 melanoma cell line was satisfactory. These findings suggest the potential of FS-TL formulation over conventional approaches in skin cancer management.

1. INTRODUCTION

Skin cancer exhibits rapid proliferation and ranks among the most prevalent malignancies globally.[1] In addition to melanoma, nonmelanoma skin cancer (NMSC) includes basal cell carcinoma and squamous cell carcinoma, which are the most often diagnosed diseases.[2] Squamous cell carcinoma is invasive in nature and malignant, which can lead to metastasis and ultimately result in the death of an individual.[3] In 2024, the American Cancer Society estimated that approximately 100,640 people in the United States suffered from a melanoma diagnosis, which ranged from about 59,170 men and 41,470 women. Tragically, melanoma was expected to exert a significant toll that year, with maximum cases indicating 8,290 fatalities—5,430 males and 2,860 females. These alarming statistics emphasized the critical necessity for increased awareness, enhanced prevention measures, and pioneering treatments to confront this persistent and formidable disease.[4] Based on a recent assessment which was conducted by the World Health Organization (WHO), India contributes to over 8% of the worldwide cancer burden, with a mortality rate of around 6%.[5] Current treatment modalities for melanoma include surgery, chemotherapeutics, radiation, biological therapy, and targeted therapy.[6]

Received: October 7, 2024
Revised: January 28, 2025
Accepted: February 5, 2025
Published: February 12, 2025

Table 1. QTPP and CQA Parameters for the Fabrication of FS-TL Formulation

QTPP	Target	Justification
Drug delivery system	Transliposome	Increased skin penetration
Release type	Sustained release	The implementation of a sustained drug release mechanism is to ensure the attainment of optimal drug concentration levels, hence facilitating the effective execution of anticancer activities.
Route of administration	Topically	This method offers targeted effects while minimizing systemic adverse reactions and increased dermal permeation.
Stability	>6 months	The drug's therapeutic efficacy should remain constant during the storage period.
CQAs	Target	Justification
Vesicle size	Less than 500 nm	Vesicles measuring under 500 nm formed a depot within hair follicles for up to 10 days, offering potential benefits for conditions affecting hair follicles requiring extended drug delivery. This finding is particularly advantageous for diseases affecting deeper layers of the skin. Moreover, over time, the administered drug tends to penetrate radially into other layers of the skin.[35]
Polydispersity index (PDI)	Less than 0.3	Liposome delivery applications possess a PDI of about 0.3 or lower is known to be assumed to reflect a homogeneous population of phospholipid vesicles.[36]
Entrapment Efficiency	Greater than 70%	Confirms an improved drug loading and enhanced therapeutic outcomes.
Zeta potential	>(±)30	Vesicles in suspension with a strongly negative or positive zeta potential will be repelled, preventing them from combining.[37]

To overcome the limitations of monotherapy, researchers are exploring strategies that avoid fixed doses, rapid titration, and inflexible designs, aiming to facilitate individualized drug adjustment for different patients.[7] Traditional monotherapy approaches indiscriminately attack actively dividing cells, eliminating both healthy and malignant cells.[8] The branch of cancer management that has gained recent attention has been combining synthetic and natural drugs. This approach offers several benefits, including targeting various cancer pathways, minimizing toxicity, and implementing a customized treatment plan for increased efficacy. In addition, combination therapy can potentially mitigate the harmful impact on healthy cells while concurrently inducing cytotoxic effects on cancer cells.[9]

5-Fluorouracil (5-FU), a well-known drug known for its potent ability to combat skin cancer, operates by impeding the process of deoxyribonucleic acid (DNA) synthesis in cancerous cells.[10] Thymidylate synthase activity is blocked to cause this inhibition, accelerating apoptosis and reducing cell growth.[11] While 5-FU's chemotherapeutic efficacy in initial cancer treatments shows a response rate of approximately 10−15%, its cytotoxic effects are amplified upon intracellular activation.[12] Active metabolites such as fluorodeoxyuridine monophosphate (FdUMP) enhance the inhibition of DNA replication, while fluorouridine triphosphate (FUTP) integrates into ribonucleic acid (RNA), impairing its synthesis and function. This dual disruption of both DNA and RNA processes effectively suppresses tumor growth while ensuring targeted action against rapidly proliferating cancer cells.[13]

In the last two decades, significant modulation strategies have been devised to enhance the tumor's responsiveness to 5-FU and to address its resistance in terms of therapeutic effectiveness. These efforts involve reducing the breakdown of 5-FU, augmenting its activation, and enhancing the activity of thymidylate synthase.[12,14] Using 5-FU with more recent chemotherapeutic agents, such as irinotecan and oxaliplatin, has enhanced response rates of 40−50%.[15] 5-FU has potent anticancer properties; however, its limited solubility limits its usage in therapeutic uses. Since 5-FU is a biopharmaceutical classification system (BCS) class III agent, in this instance, the 5-FU's low partition coefficient (−0.88) in its unbound form restricts its ability to enter the stratum corneum.[16,17]

Sesamol (SES) (5-hydroxy-1,3-benzodixole or 3,4-methylenedioxyphenol) is a secondary metabolite derived from sesame seeds (*Sesamum indicum* L.),[18] and is classified as a phenolic compound. Sesamol exhibits potential in reducing the incidence of colon cancer,[19] nonsmall cell lung cancer,[20] and malignant melanoma skin cancer,[21,22] and hepatocellular carcinoma.[23] In addition to its well-documented effects on cancer, SES has been exhaustively studied for its therapeutical properties. It has emerged as a promising metabolic regulator, harnessing its impressive role as an antimutagenic, antioxidant, anti-inflammatory, antiaging, and antihepatotoxic characteristics.[24] According to one study, sesamol reduced cytotoxicity, intracellular ROS production, lipid peroxidation, oxidative DNA damage, and apoptotic morphological alterations in human fibroblasts caused by UVB irradiation.[25] Additionally, it was discovered that sesamol reduced the expression of tyrosinase, tyrosinase-related protein-1 (TRP-1), TRP-2, microphthalmia-associated transcription factor (MITF), and melanocortin 1 receptor (MC1R) in melan-a cells, hence inhibiting melanin formation.[26]

SES demonstrates a multifaceted impact on cancer cells, inhibiting lipid peroxidation, enhancing free radical scavenging, upregulating antioxidant enzymes, suppressing pro-inflammatory cytokines, inhibiting nuclear factor kappa-light-chain-enhancer of activated B cells (NF-κB) signaling, and modulating various apoptotic and cell growth regulatory proteins, including B-cell lymphoma 2 (Bcl2), BCL2-associated X protein (Bax), tumor protein p53, caspase-3,5-lipooxygenase, and lectin-like oxidized low-density lipoprotein receptor-1 (LOX-1), presenting a potential therapeutic strategy against malignant melanoma.[27−29]

It is difficult to employ both drugs for cutaneous distribution in treating skin cancer because of their dissimilar physiochemical characteristics. Despite its favorable physicochemical characteristics, including good water solubility (38.8 ± 1.2 mg/mL) and moderate lipophilicity (log P = 1.37), sesamol faces significant therapeutic challenges. These include poor bioavailability and rapid systemic elimination, which limit its therapeutic potential.[30] Furthermore, when applied topically, sesamol's rapid transit through skin layers to systemic circulation limits its local effect on skin tissues.[31] A novel drug delivery system is being developed to address these challenges. Transitioning from oral to topical administration enhances dermal drug bioavailability and confines systemic circulation, ensuring higher drug concentration within the dermal layers. This innovative approach surpasses challenges

https://doi.org/10.1021/acsomega.4c09147
ACS Omega 2025, 10, 6857−6875

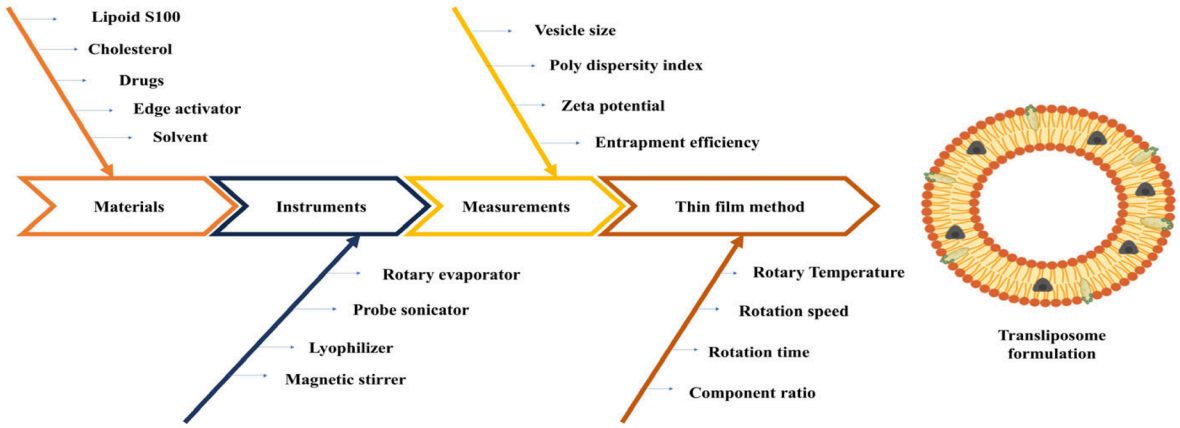

Figure 1. Risk assessment: Ishikawa diagram unveils potential influences of material and process on the properties of TL formulation.

Table 2. Study Involving the Observation of Responses in BBD to Develop FS-TL Formulations[a]

	Independent variables			Dependent variables			
Formulation batches	A: Lipoid S100 (mg)	B: Cholesterol (mg)	C: Sodium cholate (mg)	Y_1: Vesicle size (nm)	Y_2: PDI	Y_3: EE 5-FU (%)	Y_4: EE SES (%)
1	90	15	5	201.4	0.398	47.32	61.29
2	70	10	10	140.4	0.257	32.14	41.35
3	70	5	7.5	123.9	0.254	37.28	51.45
4	90	5	10	135.4	0.335	42.72	56.89
5	110	15	7.5	240.4	0.458	59.64	74.15
6	110	5	7.5	175.3	0.401	52.1	67.88
7	110	10	5	220.1	0.521	47.19	63.88
8	90	10	7.5	166.8	0.301	61.11	74.23
9	70	10	5	145.4	0.241	42.51	55.49
10	90	10	7.5	165.4	0.281	63.12	79.48
11	110	10	10	198.1	0.418	55.14	70.89
12	90	10	7.5	164.6	0.269	64.26	72.14
13	90	5	5	144.19	0.377	30.2	68.1
14	90	10	7.5	163.8	0.287	62.12	75.19
15	70	15	7.5	159.1	0.19	42.9	55.55
16	90	15	10	182.9	0.358	43.2	63.9
17	90	10	7.5	164.9	0.345	61.39	70.98

[a]The Design Expert Software was utilized to summarize various parameters for given responses (Y_1, Y_2, Y_3, and Y_4).

linked to oral drug administration, enhances patient compliance, and mitigates adverse reactions.[32]

An innovative approach was utilized to overcome the stability and encapsulation efficiency issues commonly seen in traditional liposomal delivery. The study presents a novel approach for FS-TL, that together merges the merits of liposomes as well as transfersomes for improved permeation into deeper layers of the skin for a combination impact against skin cancer. TL vehicles, enhanced with an edge activator, exhibited enhanced permeability, deposition properties, and improved solubility, drug penetration, and stability.[33,34] The potential conversion of TL in the form of a gel presents an advantageous opportunity for extended residence time at the application site and active targeting in tumor-specific dermal administration.

The present study introduces a novel approach by formulating, optimizing, and characterizing a TL gel coencapsulating 5-FU and SES for topical application, combining the chemotherapeutic properties of 5-FU with the antioxidant and anti-inflammatory benefits of SES. This innovative formulation, which enhances drug stability, skin penetration, and controlled release, represents an unexplored therapeutic strategy for localized skin cancer treatment, offering improved efficacy and reduced side effects compared to conventional therapies.

This manuscript includes optimization and various *in vitro* studies to evaluate the prepared TL. Further, *ex vivo*, dermatokinetic, penetration depth, skin interaction, and irritation studies were conducted on mice models.

2. RESULTS AND DISCUSSION

2.1. Quality by Design (QbD) Approach for Optimization. QbD is an essential step in obtaining an appropriate and dependable formulation. Table 1 presents a detailed compilation of the Quality Target Product Profile (QTPP) and the critical quality attribute (CQA) factors obtained from the QTPP. The risk assessment process utilized an Ishikawa fishbone diagram. This methodology facilitated the examination of the impact of specific variables on CQAs, as illustrated in Figure 1.

2.2. Development and Optimization of 5-FU and SES TL. The formulation of FS-TL was effectively achieved through the thin film technique followed by sonication. Subsequently, the developed formulation underwent additional optimization

https://doi.org/10.1021/acsomega.4c09147
ACS Omega 2025, 10, 6857−6875

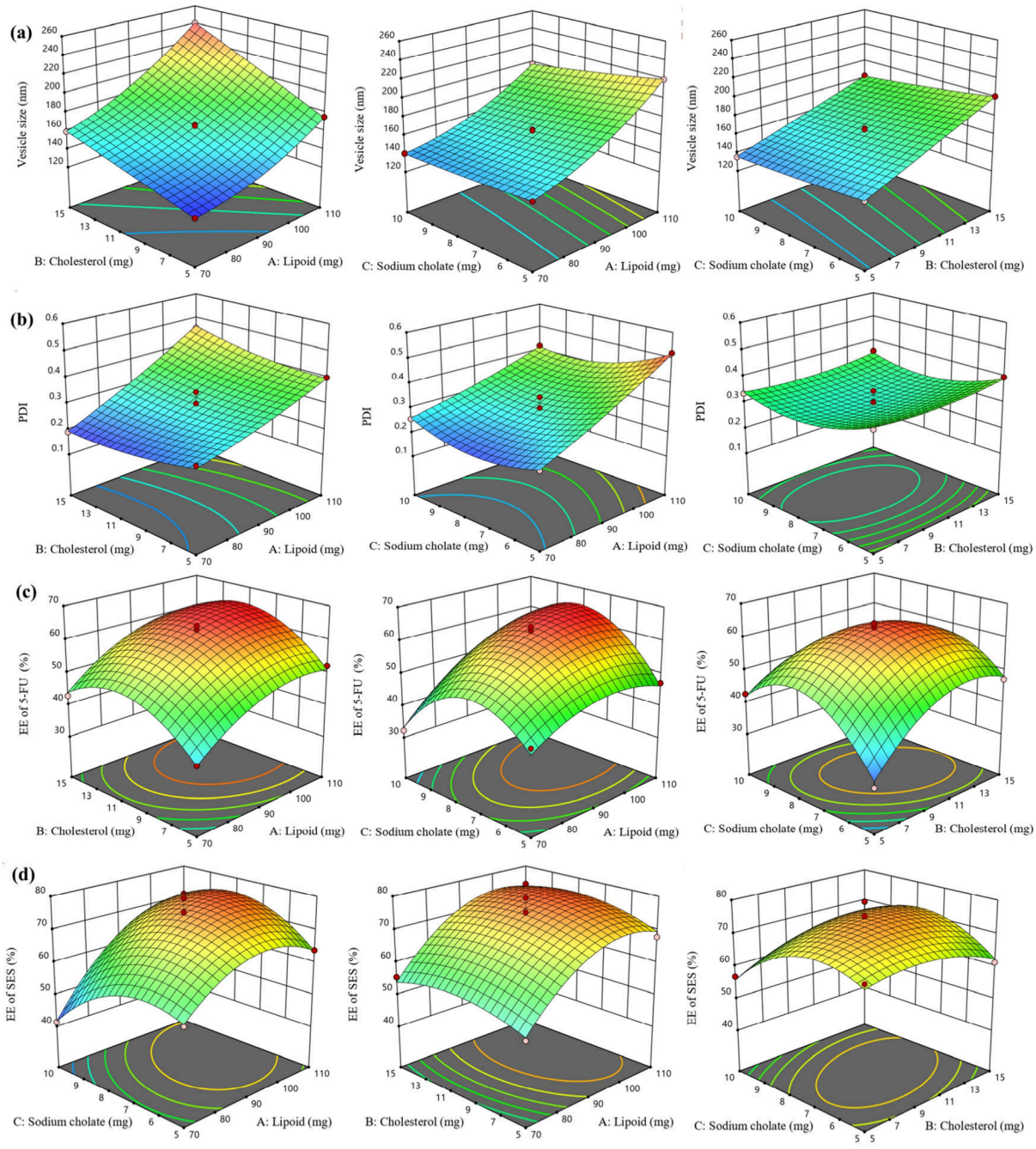

Figure 2. 3D graphs illustrate the effects of independent variables (Lipoid, cholesterol, and sodium cholate) on the dependent variables (a) Vesicle size, (b) PDI, (c) entrapment efficiency of 5-FU, and (d) entrapment efficiency of SES.

Table 3. Outcomes of the Regression Analysis Conducted on Responses Y_1, Y_2, Y_3, and Y_4

Quadratic model	R^2	Adjusted R^2	Predicted R^2	Adequate precision	SD	% CV
Response (Y_1)	0.9995	0.9989	0.9969	148.90	1.03	0.6049
Response (Y_2)	0.9679	0.9266	0.9004	17.96	0.0235	7.03
Response (Y_3)	0.9871	0.9705	0.8422	20.60	1.92	3.86
Response (Y_4)	0.9646	0.9192	0.8182	14.95	2.87	4.42

utilizing the Box Behnken design (BBD). This design involved conducting 17 experimental runs, including 5 center points, to investigate the impact of independent variables on the size (Y_1), PDI (Y_2), EE of 5-FU (Y_3), and EE of SES (Y_4) the formulation (Table 2). The connection between the independent variables and the responses was visualized through a 3D graph (Figure 2). The Polynomial quadratic model was deemed the most appropriate. The adjusted value of R^2 and the predicted value of R^2 were found to be consistent, as shown in Table 3. Additionally, all four responses exhibited a minimal lack of fit, indicating that all response surface methodology adequately fits this data.

https://doi.org/10.1021/acsomega.4c09147
ACS Omega 2025, 10, 6857−6875

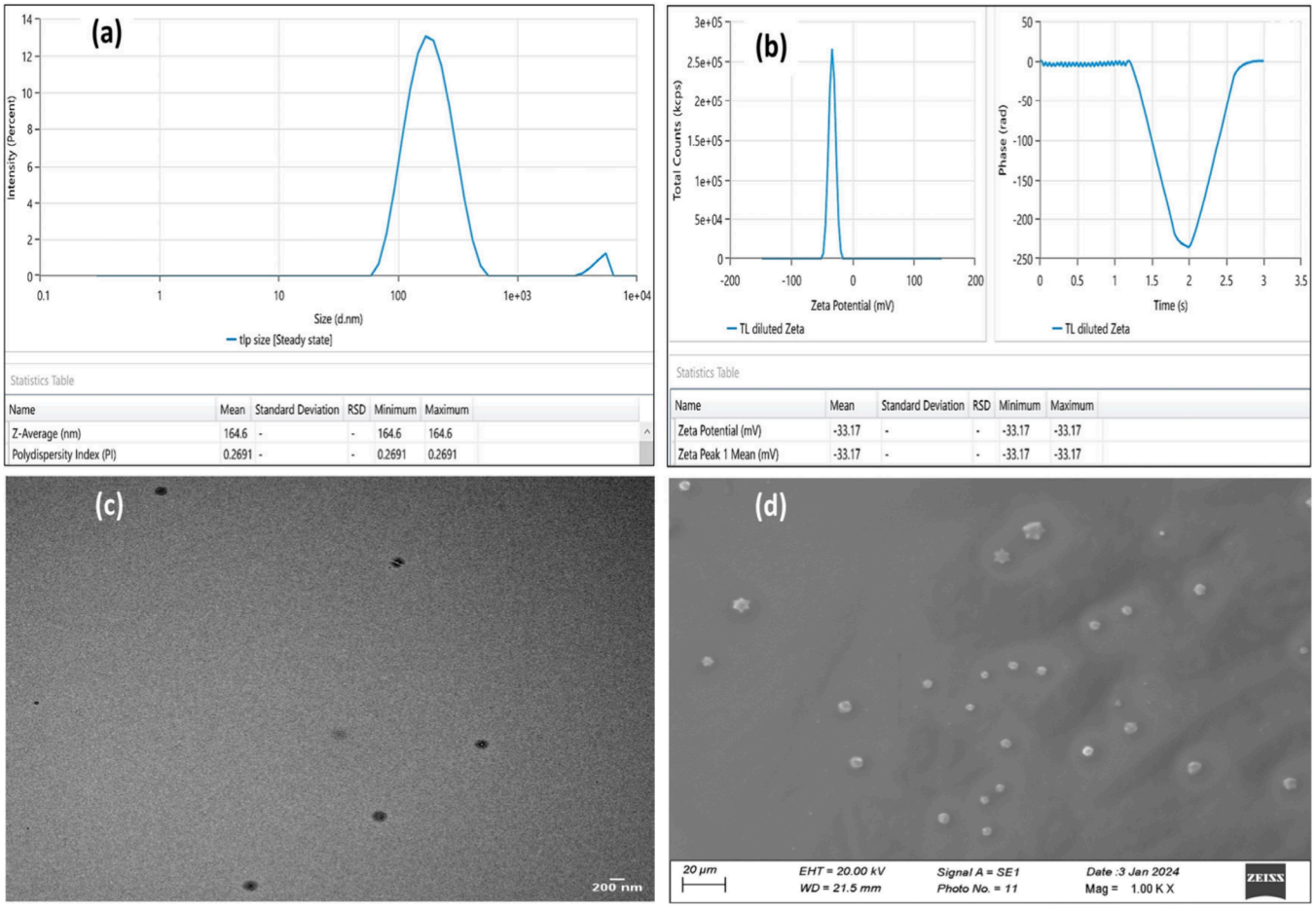

Figure 3. (a) Vesicle size, (b) zeta potential, (c) TEM, and (d) SEM images of FS-TL.

2.2.1. Polynomial Equation.

$$\text{Vesicle size} = +165.10 + 33.14A + 25.63B - 6.79C + 7.48AB - 4.25AC - 2.43BC + 9.80A^2 - 0.2263B^2 + 1.10C^2$$

$$\text{PDI} = +2.966 + 0.1070A + 0.0046B - 0.0211C + 0.0302AB - 0.0298AC + 0.0005BC + 0.0107A^2 + 0.0184B^2 + 0.0520C^2$$

$$\text{EE\%(5-FU)} = 62.4 + 7.405A + 3.845B + 0.7475C + 0.48AB + 4.58AC - 4.16BC - 5.5175A^2 - 8.9025B^2 - 12.6375C^2$$

$$\text{EE\%(SES)} = 74.404 + 9.12A + 1.32125B - 1.96625C + 0.5425AB + 5.2875AC + 3.455BC - 8.3945A^2 - 3.752B^2 - 8.107C^2$$

2.2.2. Influence of Independent Variables on Vesicle Size (Y_1). The vesicle size in the developed formulation varies between 123.90 to 240.40 nm, as indicated in Table 2. According to the mentioned polynomial equation, it was found that Lipoid S100 (A) and cholesterol (B) have a favorable impact while sodium cholate (C) has a detrimental effect on the vesicle size (Y_1) as can be seen in Figure 2a. The augmentation of lipoid S100 concentration induces the creation of a more compact matrix structure, resulting in the rigidity of the vesicles. This occurrence may be due to the increase in the size of a vesicle.[38] This phenomenon may be attributed to the ability of phospholipids to enhance drug entrapment, resulting in an expansion of the interbilayer space, and subsequently leading to an enhanced vesicle size.[39,40] The structure of cholesterol was not able to autonomously form a bilayer; instead, it becomes soluble in a bilayer of phospholipids. Elevated cholesterol levels contribute to an augmented dispersion of cholesterol molecules within the phospholipid bilayer, leading to a concomitant increase in the average diameter of the vesicle.[41] Another potential factor could be the reduction in the area per phospholipid molecule within the membrane's plane due to the thickening caused by cholesterol, leading to an overall enlargement of the vesicles.[42] On the other hand, elevated levels of sodium cholate result in enhanced emulsification and solubilization, hence causing a decrease in the dimensions of the vesicles.[43] The reduced size of the vesicle with enhancing the surfactant concentration can be ascribed to enhanced membrane flexibility and softness, leading to increased compressibility. These results align with those of the prior study by Zaki et al.[44]

2.2.3. Influence of Independent Variables on PDI (Y_2). The PDI in the developed formulation varies between 0.190−0.521, as indicated in Table 2 and Figure 2b. The equation provided above illustrates that the inclusion of lipoid S100 (A) and cholesterol (B) has a positive impact on PDI, as evidenced by the report in Figure 2b. The augmentation of lipoid S100 and cholesterol quantities from 70 to 110 mg and 5 to 15 mg, respectively, led to an elevation in the PDI. The observed decrease in PDI was attributed to the higher concentration of

https://doi.org/10.1021/acsomega.4c09147
ACS Omega 2025, 10, 6857−6875

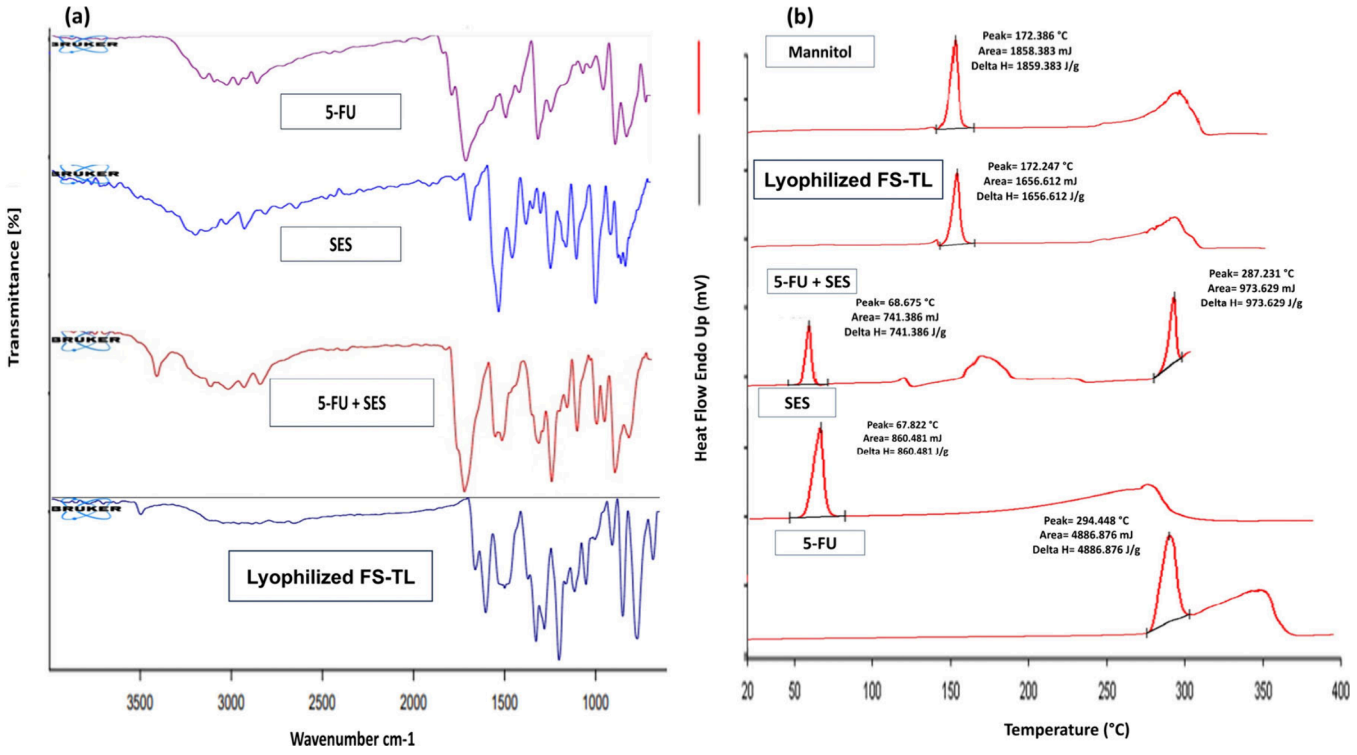

Figure 4. (a) FTIR spectra of 5-fluorouracil (5-FU), sesamol (SES), physical mixture of 5-FU and SES, and lyophilized FS-TL and (b) DSC thermograms of mannitol, lyophilized FS-TL, physical mixture of 5-FU and SES, sesamol (SES), and 5-fluorouracil (5-FU).

sodium cholate (C). The aforementioned observation implies that the preservation of a constant size distribution is known to be crucial to minimizing interfacial tension and attaining a homogeneous TL structure.[45]

Influence of Independent Variables on EE% (Y_3 and Y_4). Based on Table 2, the developed formulation has an entrapment efficiency of 30.2 to 64.26% for 5-FU (Y_3) and 41.35 to 79.48% for SES (Y_4). The polynomial equation shown above reveals that Lipoid S100 (A) and cholesterol (B) have a beneficial influence on the entrapment efficiency (Y_3 and Y_4), whereas sodium cholate (C) has a negative impact on the EE of 5-FU and SES (Y_3 and Y_4) as depicted in Figure 2c,d. The ability of TL to efficiently encapsulate a substantial amount of the drug is regarded as a critical factor for achieving optimal topical administration. The increase in entrapment efficiency percentage with higher lipoid S100 concentration may be linked to the expansion of the bilayer's domain size due to the formation of more TL vesicles. Consequently, this phenomenon facilitates an increased potential for trapping of 5-FU and SES within the TL vesicles. To facilitate the establishment of stable vesicles, the formulation was engaged with cholesterol. In this case, cholesterol's main functions are to stop leaks, make bilayers more stable, and make it harder for solutes in the vesicles' aqueous core to be absorbed.[33] The inclusion of cholesterol has been found to enhance the encapsulation effectiveness of TL. This improvement can be attributed to the increased affinity between phospholipid molecules and the heightened stiffness of the transliposomal membrane.[46] However, the entrapment effectiveness of TL vesicles is reduced as the concentration of sodium cholate is enhanced from 5 to 10 mg. The decrease in entrapment efficiency seen at elevated concentrations of sodium cholate may stem from a mechanism where, beyond a certain threshold concentration, sodium cholate impacts the stability (structural) of the vesicle bilayer membrane. This disruption leads to the release of drugs from the vesicular structure, thereby diminishing drug encapsulation.[47]

2.3. Validation of Design. The utilization of BBD was employed to attain the optimal formulation characterized by reduced vesicle size and polydispersity index (PDI), as well as enhanced entrapment efficiency. Hence, FS-TL formulations were developed using process factors, the runs, and responses specified in Table 3. The experimental data retrieved from the desired formulations were subsequently subjected to a comparison with the predicted responses. The high level of resemblance between the predicted and experimental values indicates the efficacy and precision of the optimization approach. The study determined that the desirability ratings assigned to responses were consistently rated as 1, suggesting a high level of desirability. These responses were associated with a very low level of prediction error.

2.4. Optimized Formulation. The optimal formulation determined using the Box-Behnken design (BBD), consisted of lipoid S100 (87.53 mg, A), cholesterol (7.67 mg, B), and sodium cholate (7.23 mg, C). This formulation was further characterized for various characteristics.

2.5. Characterization of FS-TL. *2.5.1. Determination of Vesicle Size and PDI.* Assessing PDI and the vesicle size is crucial for the evaluation of the quality of transliposomal formulations. The optimized formulation displayed a vesicle size of 165.6 ± 1.1 nm, and a PDI of about 0.28 ± 0.01, as depicted in Figure 3a. The size of vesicles and the PDI have the potential to impact the release and absorption of loaded drugs upon reaching the intended site, hence directly influencing their pharmacological properties. A decrease in the size of vesicles and PDI indicates a more uniform and presumably more stable transliposomal formulation.[48] The size of the vesicle is crucial in influencing its permeability, the drug release

https://doi.org/10.1021/acsomega.4c09147
ACS Omega 2025, 10, 6857−6875

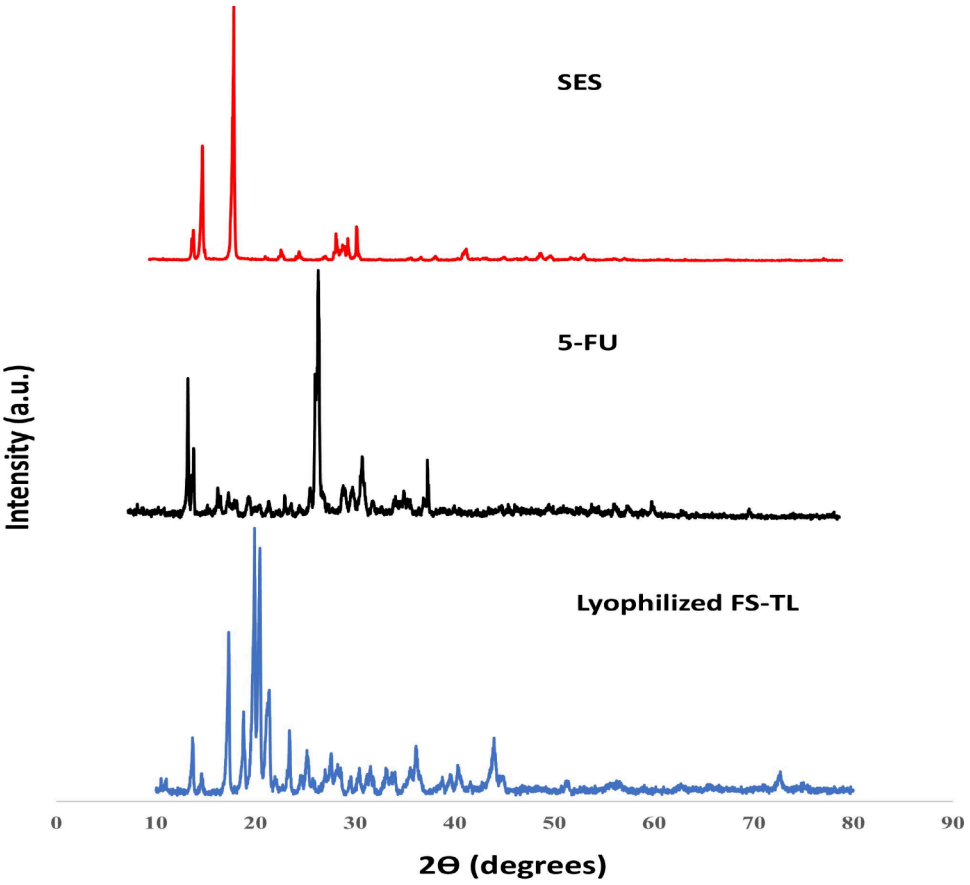

Figure 5. XRD spectra of sesamol (SES), 5-fluorouracil (5-FU), and lyophilized FS-TL.

from the formulation, and its stability aspects. Furthermore, it exerts an impact on the passive targeting of neoplastic cells. The vasculature of the tumor exhibits a wide range of sizes, significant heterogeneity, increased permeability, and a propensity for leakage. The permeable nature of skin tumor cells facilitates the infiltration of nanovesicles via the enhanced permeability retention (EPR) effect.[49] The nanosystem, characterized by its sub-200 nm vesicle size, demonstrates a high capability to efficiently infiltrate tumor cells through the EPR effect.[36] The PDI is a measure used to describe the size distribution of nanovesicles. An acceptable PDI score of 0.3 or below suggests a homogeneous phospholipid vesicle population.[50]

2.5.2. Zeta Potential of FS-TL. The zeta potential magnitude offers valuable data based on the potential stability of the colloidal system. When the zeta potential of all suspended particles is significantly negative or positive, they will exhibit a mutual repulsion, hence preventing any inclination for vesicle aggregation.[51] Vesicles with more negativity or positivity value of zeta potential are typically regarded as being in a stable state.[52] The zeta potential of FS-TL was determined to be −33.17 ± 0.9 mV, as illustrated in Figure 3b. The presence of a negative surface potential showed promise in facilitating the improved penetration of the drug following its application to the skin.[53] The attainment of appropriate zeta potential is a crucial factor in the optimization of nano drug delivery, as it exerts influence on targeted therapeutic outcomes, stability, and the profile of drug release.[37]

2.5.3. Assessment of EE and Drug Loading. The measures of these parameters are essential indicators that reflect the quality of TL. The % EE for 5-FU and SES was found to be 63.16 ± 1.07% and 75.60 ± 3.68%, respectively. The drug loading% for 5-FU and SES was found to be 5.87 ± 0.099% and 7.03 ± 0.34%, respectively. The behavior can primarily be attributed to interactions between the drugs and the lipid bilayers.[54]

2.5.4. Morphology Studies. Transmission electron microscope (TEM) provides detailed insights into the surface properties of FS-TL, as shown in Figure 3c. The images confirmed the formulation's spherical morphology and well-defined vesicular structure, indicative of solid particulate properties. Similarly, scanning electron microscopy (SEM) results, depicted in Figure 3d, revealed spherical vesicles, focusing on surface characteristics and further supporting the structural consistency of the formulation.

2.6. Compatibility Studies. *2.6.1. Fourier Transform Infrared (FTIR).* The study used Fourier Transform Infrared (FTIR) spectroscopy to determine possible interactions between the drugs as well as the excipients in the formulation. In Figure 4a, distinct peaks corresponding to specific functional groups of 5-FU and SES were observed, confirming their presence within the formulation. For 5-FU, notable peaks included the C═O at 1642.18 cm^{-1}, N−H at 3119.67 cm^{-1}, C−F at 1416.73 cm-1, C−N at 1246.87 cm^{-1}, and pyrimidine compound at 1341.88 cm^{-1}.[55] Similarly, for SES, peaks such as disubstitution of phenyl at 737.86 cm^{-1}, C−H bonding bands at 833.27 cm^{-1}, symmetric (═C−O−C stretching) at 1026.20 cm^{-1}, C−O−C stretching at 1084.73 cm^{-1}, CH_2 bending at

https://doi.org/10.1021/acsomega.4c09147
ACS Omega 2025, 10, 6857−6875

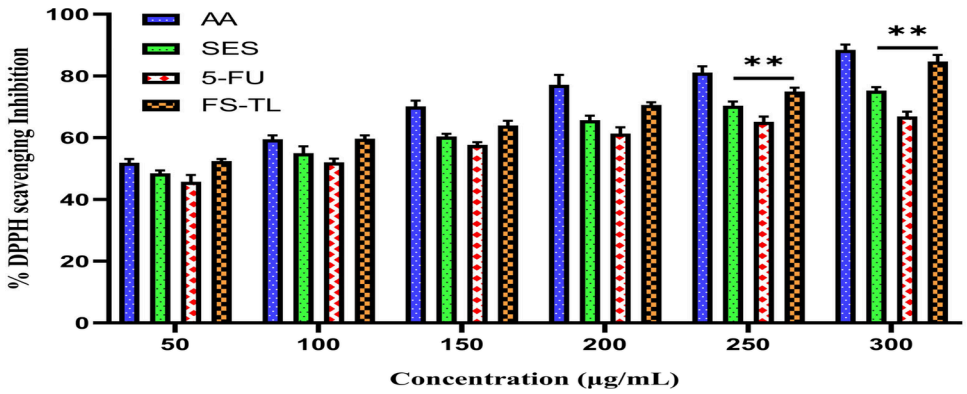

Figure 6. Comparative percentage of DPPH radical scavenging activity (% inhibition) for ascorbic acid (AA), Sesamol (SES), 5- fluorouracil (5-FU), and FS-TL at concentrations ranging from 50 to 300 μg/mL ($p < 0.0001$, $n = 3$).

1463.93 cm^{-1}, CH bending of phenyl group at 1388.31 cm^{-1}, phenyl skeletal frequency at 1625.26 cm^{-1}, and unsaturated −CH at 3171.80 cm^{-1} were identified.[56] Additionally, analysis of the developed FS-TL formulation revealed no observable interactions. A comparison of the FTIR spectra of the drugs, their combination, and the transliposomal formulation indicated efficient encapsulation of the drugs within the lipids, highlighting the compatibility of the optimized formulation.

2.6.2. Differential Scanning Calorimetry (DSC). According to the reported data, the melting point range of 5-FU and SES has been documented to be between 282 °C[55] and 65.3 °C.[57] Figure 4b displays the DSC thermogram of pure drug SES, 5-FU, a combination of both drugs, drug-loaded formulation FS-TL, and pure mannitol. Upon doing a DSC analysis of the pure 5-FU and SES, it was noted that a distinct endothermic peak occurred at a temperature of 294.44 and 67.82 °C, respectively and there was no significant change in the peaks of both drugs were observed in combination. This observation serves as confirmation of the drug's purity and crystalline characteristics. The DSC-based thermogram of FS-TL displayed a distinct, well-defined endothermic peak at 172.24 °C, indicative of the presence of mannitol, aligning with the peak observed in pure mannitol. The conversion of a substance from a crystalline form to an amorphous nature is only indicated by the presence of a peak corresponding to mannitol. Additionally, it demonstrates the comprehensive encapsulation of the drugs, with no observed instances of drug precipitation.

2.6.3. X-ray Diffraction (XRD) Analysis. The X-ray diffraction (XRD) spectra exhibited discernible peaks corresponding to 5-FU at diffraction angles of 16.5°, 19.3°, 31.48°, and 39.4°. Additionally, recognizable peaks of SES were observed at diffraction angles of 15.4°, 20.19°, and 30.49°, it is evident that 5-FU and SES, both are present in a crystalline powder (Figure 5). Nevertheless, the diffraction pattern of the drug-encapsulated FS-TL, does not exhibit any comparable diffraction peaks for 5-FU and SES. The results suggest that both drugs were evenly distributed within FS-TL, resulting in their entrapment in an amorphous state. The same outcome was likewise noted when drugs were enclosed within the nano formulation.[58]

2.7. Antioxidant Activity. The study sought to elucidate the antioxidant potential of drug samples across a range of concentrations, crucial for understanding their therapeutic efficacy. Results revealed a significant positive correlation between concentration and antioxidant activity, underscoring the importance of dosage optimization in maximizing therapeutic benefits. At the highest concentration of (300 μg/mL), ascorbic acid (AA) showed the most pronounced antioxidant activity (88.42 ± 1.70%) followed closely by the FS-TL (84.67 ± 2.3%). In comparison, SES exhibited 75.25 ± 1.1%, and 5-FU showed the lowest inhibition among the sample (66.88 ± 1.5%). Notably, the radical scavenging capability of the sample of FS-TL, when used at its greatest concentration of 300 μg/mL, was shown to be similar to the antioxidant capacity of AA at a similar concentration as shown in Figure 6. Vesicular encapsulation might perhaps explain this phenomenon due to the enhanced solubility and dispersion of drugs. The results validate that the vesicle formulation successfully preserved the antioxidant activity of the drugs.

Samples that have lower half-maximal inhibitory concentration (IC_{50}) values indicate a more pronounced level of antioxidant activity. The IC_{50} values for the standard sample (AA), 5-FU, and SES were 28.19 μg/mL, 79.27 μg/mL, and 56.88 μg/mL, respectively. The combination ratio of 5FU and SES in a 1:1 ratio was chosen due to its superior efficacy, as shown by its lowest IC_{50} value compared to alternative ratios.

2.8. Combination Index. The Combination Index (CI) for the drug ratio was 0.911, which is less than 1. This result validates the synergistic interaction between the drugs, reinforcing the rationale for their combined use in this specific ratio for optimal therapeutic outcomes.

Given the detrimental effects of UV radiation-induced oxidative stress, such as sunburn, accelerated aging, and the formation of tumors, the antioxidant properties of compounds like 5-FU and SES hold immense therapeutic potential.[59,60] This study offers critical insights into their antioxidant mechanisms, opening new avenues for the development of innovative therapeutic strategies aimed at combating oxidative stress-related disorders.

2.9. Drug Release (*In Vitro*). The comparative drug release profiles of 5-FU and SES from the FS suspension and the FS-TL formulation were evaluated using a dialysis bag. The FS suspension exhibited a rapid release, with 82.88 ± 0.64% of 5-FU and 80.15 ± 0.24% of SES released within 4 h. Conversely, the FS-TL formulation displayed a significantly slower release, with only 29.82 ± 1.2% of 5-FU and 28.62 ± 1.5% of SES released during the same 4 h. However, over 24 h, the FS-TL formulation demonstrated a sustained release, with 82.52 ± 1.21% and 86.17 ± 1.0% release for 5-FU and SES, respectively. This biphasic release pattern included an initial accelerated release phase within the first 4 h, attributed to the desorption of loosely bound drug molecules and release from

https://doi.org/10.1021/acsomega.4c09147
ACS Omega 2025, 10, 6857−6875

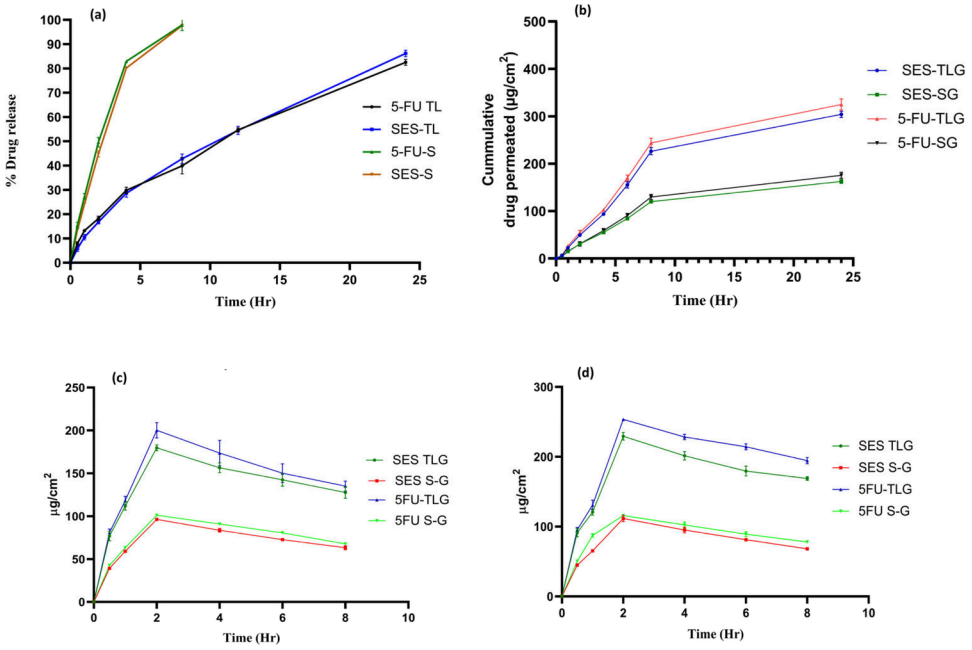

Figure 7. Comparative analysis of 5-fluorouracil (5-FU) transliposome (5-FU-TL) and sesamol (SES) transliposome (SES-TL) formulations, along with 5-fluorouracil suspension (5-FU-S-G) and sesamol suspension gel (SES-S-G). (a) *In vitro* drug release over time for both formulation and suspension. (b) *Ex vivo* permeation through mouse skin for gel formulations and suspensions. (c) Drug present in the epidermis. (d) Drug present in the dermis.

the transliposomal surface, followed by a slower, sustained release phase, likely due to the elasticity of vesicles induced by edge activators while maintaining vesicle integrity.[61,62]

The larger vesicle size in the FS suspension contributed to its less effective membrane permeation compared to the transliposomal formulation. The smaller vesicle size of the FS-TL formulation enhanced drug diffusion and provided sustained release, reducing systemic absorption and minimizing potential systemic side effects.[63,64] The release kinetics of FS-TL were evaluated using various release models, including Higuchi (R^2 = 0.9961), zero-order (R^2 = 0.9523), first-order (R^2 = 0.9922), and Korsmeyer-Peppas models (R^2 = 0.9935). Based on the analysis, it can be concluded that the Higuchi model is the most appropriate for describing drug release behavior. Additionally, the release mechanism from the FS-TL formulation follows a Korsmeyer-Peppas diffusion process, which is characterized by non-Fickian diffusion.

2.10. Skin Permeation (*Ex Vivo*). The investigation on permeation via the mice skin showed that the 5-FU-SES conventional gel had a cumulative drug permeation of 175.28 ± 6.41 $\mu g/cm^2$ for 5-FU and 162.55 ± 4.07 $\mu g/cm^2$ for SES. On the other hand, the FS-TLG exhibited a higher drug permeation rate of 324.92 ± 11.57 $\mu g/cm^2$ for 5-FU and 304.12 ± 6.74 $\mu g/cm^2$ for SES via the skin, as depicted in Figure 7b. The primary factor leading to an enhanced permeation was the occlusive behavior exhibited by the TL gel nanosystems. This behavior caused a modification in the arrangement of corneocytes and the widening of intercorneocyte openings through skin hydration. As a result, there was an increased amassing of nanoscale drug carriers in the epidermis as well as dermis layers of the skin.[65] Moreover, due to their strong affinity for biological made-up membranes, the phospholipid bilayers found in vesicles interact with the skin, thus increasing its permeability.[66] Apart from that, the presence of sodium cholate in the TL formulation works as an edge activator. As edge activators, these substances could augment the permeation of vesicles across the dermal pores by promoting vesicular deformability. Enhancing the flexibility of vesicles increases their ability to hold and bind water when applied without occlusion. This, in turn, improves the integration of vesicles into the stratum corneum lipid layer, ensuring optimal hydration conditions.[67]

2.11. Dermatokinetics. The dermatokinetic investigation results revealed significantly higher concentrations of 5-FU and SES from FS-TL gel (FS-TLG) in the epidermis and dermis regions of the skin compared to those found in the FS-suspension gel ($p < 0.001$), as depicted in Figure 7c,d. An investigation using noncompartmental methods revealed that the FS-TLG had a greater maximum concentration ($C_{skin\ max}$) and the area under the curve (AUC_{0-8}) compared to the FS-Suspension gel. The concentration of drug accumulation in the intended area of the skin was shown to be higher in the developed gel formulation compared to the suspension gel (Table 4). The findings on TL delivery indicate a substantial increase in the permeation mechanism when administered via a topical route. The current observation could be linked with some previously reported outcomes of the skin permeation study and confocal laser microscopic analysis. These studies demonstrated an augmented penetration of the formulation, which can be attributed to the formulation's elasticity as well as the presence of an edge activator and phospholipid.

2.12. Skin Interaction. In the study, the thermal properties of mice skin were assessed by measuring the transition midpoint (Tm) and enthalpy (ΔH) values using DSC (Figure 8). The untreated mice's skin exhibited a Tm value of 143.36 °C and an ΔH value of 446.31 J/g. In comparison, the treated mice showed a reduced Tm value of 76.6 °C alongside an elevated ΔH value of 966.185 J/g. This decrease in Tm values in treated skin suggests a potential alteration in the lipid bilayer's phase transition temperature.

https://doi.org/10.1021/acsomega.4c09147
ACS Omega 2025, 10, 6857−6875

Table 4. Dermatokinetic Parameters (Epidermis (EPI) and Dermis (DER)) of Suspension and FS-Loaded TL Gel and FS-Suspension Gel

Dermatokinetic parameters	Suspension gel 5-FU (5FU-SG)		Suspension gel SES (SES-SG)		5-FU-TLG		SES-TLG	
	EPI	DER	EPI	DER	EPI	DER	EPI	DER
$T_{skin\ max}$ (hr)	2	2	2	2	2	2	2	2
C_{skin} max (μg/cm^2)	101.18 ± 0.921	115.78 ± 1.11	96.24 ± 1.39	111.64 ± 4.39	200.15 ± 8.92	253.53 ± 1.49	179.8 ± 3.44	229.4 ± 5.38
AUC_{0-8} (μg/cm^2 h)	665.27 ± 38.61	725.59 ± 18.76	584.06 ± 7.54	660.03 ± 13.05	1203.56 ± 77.69	1605.91 ± 24.36	1095.08 ± 74.00	1403.47 ± 30.9
Ke (h^{-1})	0.069 ± 0.003	0.070 ± 0.007	0.069 ± 0.015	0.081 ± 0.010	0.071 ± 0.013	0.042 ± 0.002	0.05 ± 0.002	0.056 ± 0.02

Furthermore, the untreated skin displayed a second peak at 312.30 °C with an ΔH 296.34 J/g. In contrast, the treated skin demonstrated a second peak at 320.466 °C with an ΔH of 36.82 J/g. The increase in Tm values in the treated skin implied a potential alteration in the lipid bilayer's phase transition temperature. Concurrently, the decrease in ΔH values suggests heightened enthalpy during this phase transition.[68] These findings may indicate changes in lipid bilayer structure, while an enhancement in lipid bilayer fluidity is induced by the application of FS-TLG. Such alterations in skin thermal properties may have implications for the permeation and absorption of drugs, influencing the efficacy and delivery of the formulated drugs.

2.13. Confocal Laser Scanning Microscopy (CLSM). The utilization of CLSM is a common and effective technique for visualizing the degree of penetration achieved by nanocarriers. The CLSM images depicted that the hydro-alcoholic solution containing Rhodamine B penetrated the skin to a depth of only 10.0 μm, as illustrated in Figure 9a. This observation indicates that the solution was confined solely to superficial layers of the skin. While, in contrast, the TLG formulation containing a rhodamine dye exhibited a notable permeation capacity of up to 30.0 μm, as depicted in Figure 9b, thus demonstrating an increased ability to penetrate. These findings are in line with previous research.[33]

2.14. Skin Irritation. The control group, positive control group, and FS-TLG were evaluated for skin irritation using erythema and edema ratings. Erythema scores for the control group (0.0 ± 0.0), positive control group (3.49 ± 0.55), and FS-TLG (0.47 ± 0.11) were recorded, respectively. Similarly, the edema scores for these groups were 0.0 ± 0.0, 3.87 ± 0.66, and 0.51 ± 0.09, respectively. It is important to mention that compounds with scores of 2 or below are classified as nonskin irritants. The data indicates that the FS-TLG formulation yielded scores below 2 for both erythema and edema, suggesting nonirritant properties. Therefore, the developed FS-TLG demonstrates no skin irritancy based on dermal irritation data, as illustrated in Figure 10.

2.15. Cytotoxicity. The efficacy of FS-TL and FS-suspension was assessed *in vitro* by measuring the percentage of cytotoxicity on the A431 cell line, with results depending on the concentration of the test samples (Figure 11). At the highest concentration of 300 μM, the cytotoxicity percentage was 90.38 ± 0.93% for FS-TL and 77.60 ± 1.00% for FS-Suspension. A significant difference by comparing the outcomes of cells treated with FS-TL and FS-suspension ($p < 0.05$). The IC_{50} values, which indicate the concentration at which 50% of cell toxicity is reached, were found to be 70.24 ± 2.84 μM for FS-TL and 146.177 ± 2.29 μM for FS-suspension. The superior effectiveness of FS-TL can be attributed to the increased sensitivity of malignant cells to 5-FU and SES, causing inhibition of cancer cell growth as well as induction of apoptosis, more so than the FS-suspension. These findings align with previous research demonstrating the cytotoxic properties of 5-FU and SES nanoformulations against various cancer cell lines, including A431 and SK-MEL-24 melanoma cell lines.[22,69]

2.16. Stability Studies. Table 5 illustrates the stability of FS-TL under storage conditions. According to the results, vesicle size, PDI, and zeta potential remained consistent at 4 °C, over the 6 months research period, formulation demonstrating excellent stability.

https://doi.org/10.1021/acsomega.4c09147
ACS Omega 2025, 10, 6857−6875

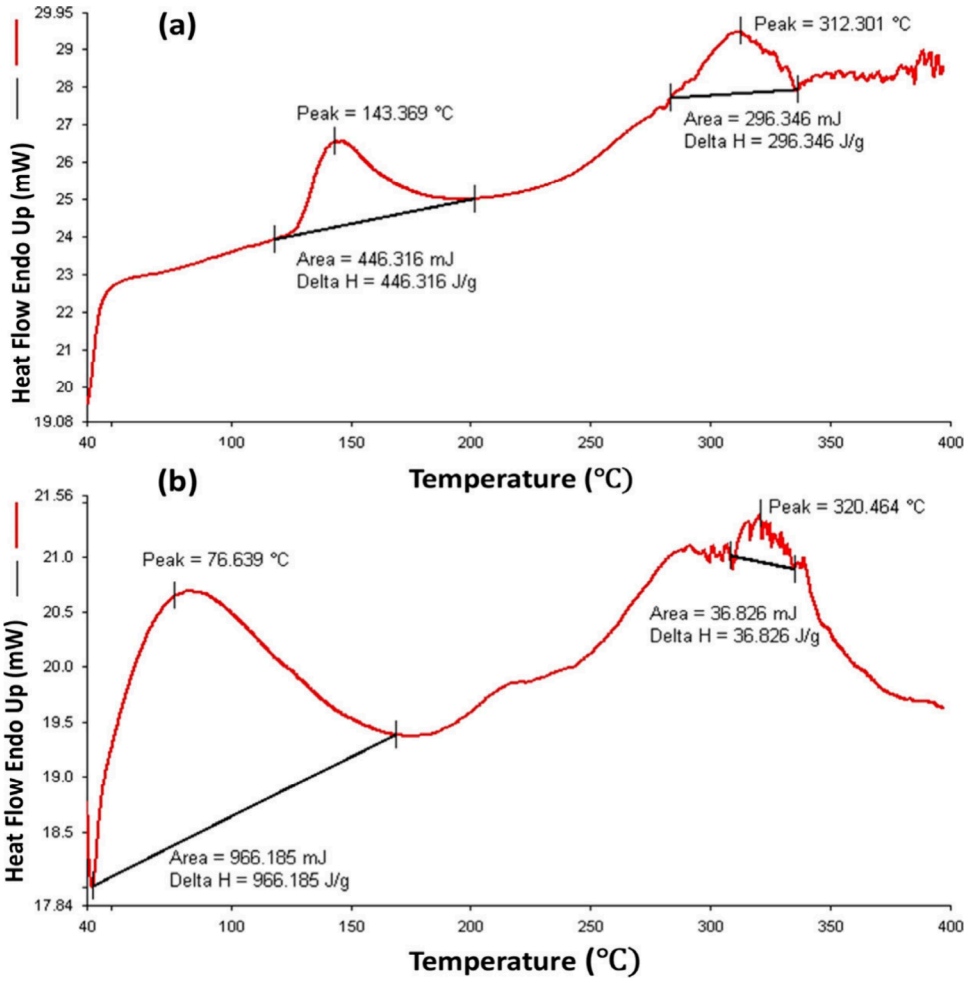

Figure 8. DSC thermograms of mice's skin (a) untreated, and (b) treated with FS-TLG.

3. CONCLUSION

The nanoformulation of 5-FU and SES-loaded transliposomal gel shows potential for skin cancer management. The formulation, optimized using BBD, has favorable characteristics, including appropriate vesicle size, and zeta potential with a high entrapment efficiency. *In vitro* drug release, *ex vivo* skin permeation, and dermatokinetic investigation show significant drug delivery to both epidermis and dermal layers. The interaction of the formulation with the skin, enhanced permeation, and reduced irritation indicate its safety for clinical use. Overall, based on the comprehensive evaluation, it was concluded that the optimized FS-loaded transliposomal gel formulation offers superior potential compared to its conventional formulation, highlighting its promise for enhanced efficacy and reduced toxicity in the management of skin cancer. Additionally, comprehensive animal studies will be conducted to assess the transliposomal gel's efficacy in inhibiting tumor growth and evaluating parameters such as tumor size, and histopathological characteristics. These investigations aim to authenticate the translational capability of this formulation for effective skin cancer management.

4. EXPERIMENTAL SECTION

4.1. Materials. 5-FU (≥99% purity (HPLC) was obtained from Otto Pharmaceutics Pvt Ltd. in India, while Sesamol (≥98% purity), cholesterol, and sodium cholate (≥97% purity) were sourced from Sigma-Aldrich Pvt Ltd. in Mumbai, India. Lipoid S100 was acquired from Lipoid SD. Rhodamine B, ascorbic acid, and 2,2-diphenyl-1-picrylhydrazyl (DPPH) were procured from Sigma-Aldrich in Mumbai, India. Carbopol 940, triethanolamine (≥99% purity), and polyethylene glycol (PEG) were bought through Unicure India Ltd. in Noida, India. Mannitol was obtained from SD Fine-Chem Ltd. in Mumbai, India. Other laboratory-grade materials such as methanol, ethanol, etc., were sourced from SD Fine Chemical Ltd. in Mumbai.

4.2. Quality Target Product Profile. A comprehensive Quality Target Product Profile (QTTP) was conducted to ensure the safety and efficacy of a prepared formulation. Apart from serving as a strategic framework, this QTTP is intended to support the integration of Quality by Design (QbD) principle that would also promote a systematic approach to the formulation development process.[70] This QTTP outlines the essential performance characteristics required of the finished product. Through QbD, attention is directed toward critical quality attributes (CQAs) that significantly impact formulation quality. Variability in these CQAs is often influenced by some Critical Process Parameters (CPPs) that usually link to various development processes as well as Critical Material Attributes (CMAs) concerning formulation composition. To thoroughly assess potential factors affecting formulation quality, a series of risk assessment studies were conducted, drawing upon a range of techniques outlined in the ICH Q9 guidelines.[71] The

https://doi.org/10.1021/acsomega.4c09147
ACS Omega 2025, 10, 6857−6875

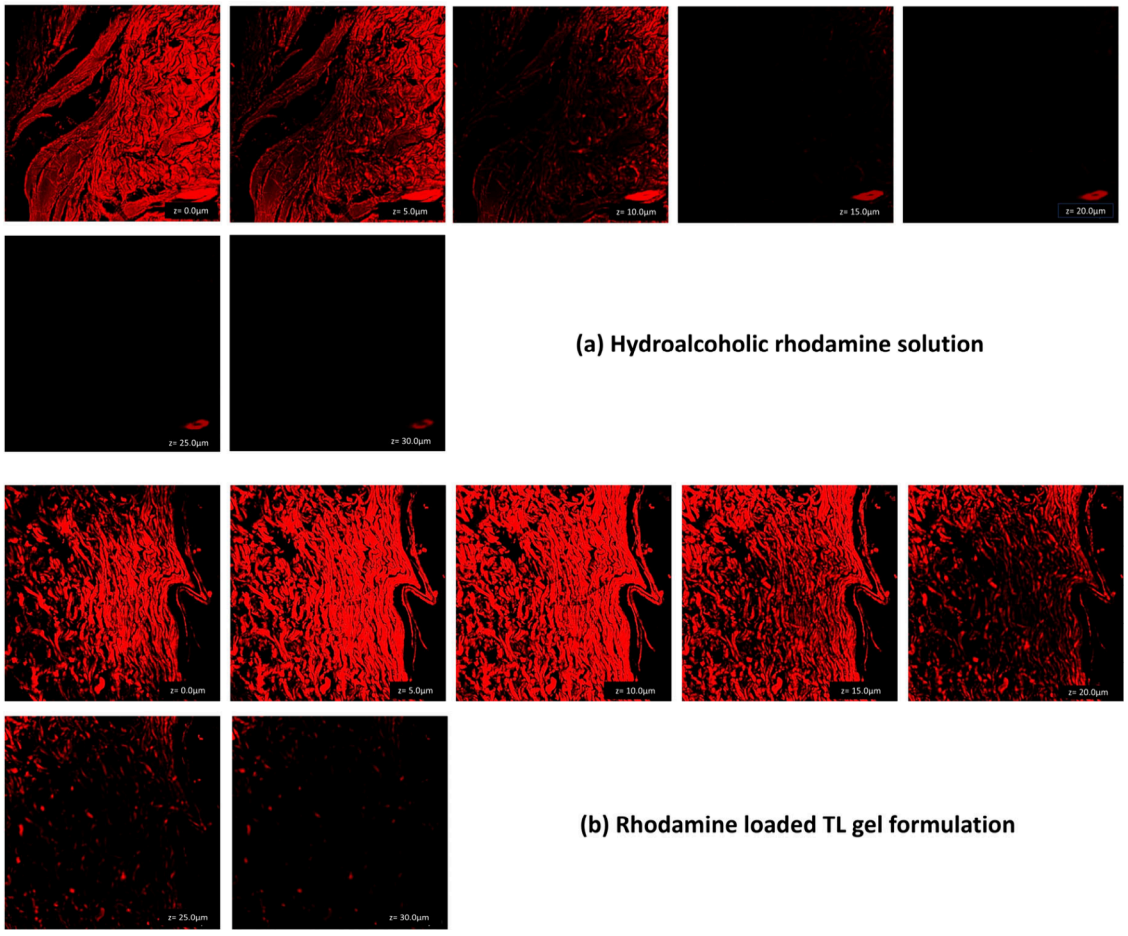

Figure 9. Comparative CLSM image of (a) hydroalcoholic solution and (b) TL formulation gel across the excised mice skin

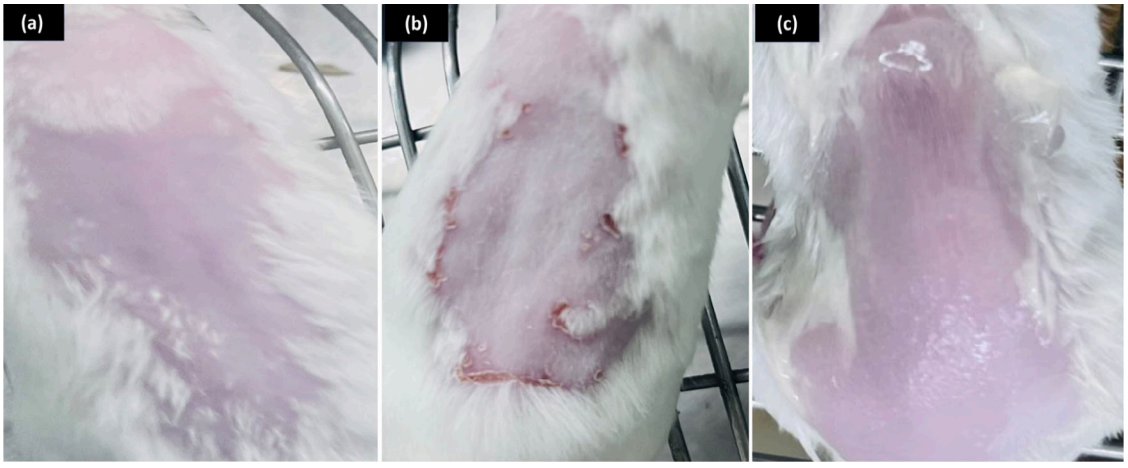

Figure 10. Skin irritation images of mice (a) normal control, (b) treated with positive control (formalin solution), and (c) FS-TLG formulation.

Ishikawa Fishbone Diagram, Failure Mode and Effects Analysis (FMEA), and Fault Tree Analysis are frequently used tools. In this investigation, a methodology utilizing the Ishikawa Fishbone Diagram has been recently adopted to explore the cause-and-effect relationships among various components.

4.3. Development of 5-FU- and SES-Loaded Transliposomes (FS-TL). The process of developing TL involved a thin-film method followed by sonication. In a 2:1 v/v solution of chloroform and methanol, the lipid consisting of lipoid S100, cholesterol, sodium cholate, and sesamol were meant to be dissolved. To evaporate the organic phase, the solution was put into a round-bottom flask and run through a rotary evaporator (Model Eyela N-1000 series, Tokyo Rikikikai Co., Ltd., Japan). The thin film thus obtained was dried and later rehydrated with phosphate-buffered saline (PBS) at 150 rpm which included 5-FU at a pH of 5.5. To generate a nanovesicle, the formulation was followed by sonication for two minutes with the help of a probe sonicator (UP100H, Hielscher, Germany).[72]

https://doi.org/10.1021/acsomega.4c09147
ACS Omega 2025, 10, 6857−6875

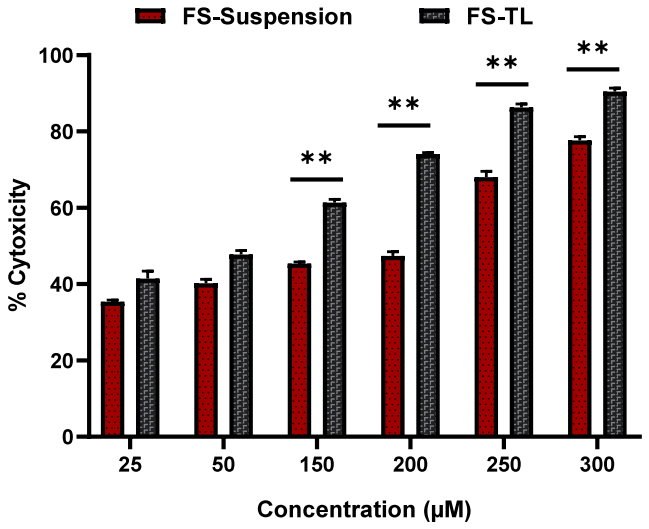

Figure 11. % Cytotoxicity of FS-TL and FS-suspension on the A431 cell line, as evaluated via the MTT assay ($p < 0.05$).

4.4. Optimization of FS-TL. The preformulating investigation was carried out to explore the influence of various independent factors on the dependent variables, such as the amounts of lipoid S100 concentration (mg, A), cholesterol (mg, B), and sodium cholate concentration (mg, C). These studies aimed to evaluate vesicle size (Y_1), PDI (Y_2), and entrapment efficiency (% EE; Y_3, and Y_4). Employing a Box-Behnken design (3-factor), the impact of the three independent variables was optimized. The collected runs were analyzed via Design of Experiment version 13 software (Stat-Ease), and the significance of each element and their interactions was determined through analysis of variance (ANOVA). Table 6 outlines the selected upper and lower bounds for the experimental design, providing a comprehensive framework for the research process.

4.5. Characterization of FS-TL. *4.5.1. Measurement of Vesicle Size, PDI, and Zeta Potential.* Vesicle size, PDI, and zeta potential of the FS-TL formulation were determined at a temperature of 25 °C with the help of dynamic light scattering (DLS) and a Malvern zeta sizer instrument (Malvern Instrument, U.K.). To reduce the occurrence of multiple scattering phenomena due to interparticle interaction, formulation dispersion was diluted 10-fold using deionized water.[73]

4.5.2. Assessment of the EE and Drug Loading. The % EE of FS-TL was determined with the help of the ultracentrifugation technique, followed by filtration. The FS-TL

Table 6. Dependent and Independent Variables Utilized in the FS-TL Using BBD

Independent Variable	Levels		
	Minimum	Moderate	Maximum
A = Lipoid S100 (mg)	70	90	110
B = Cholesterol (mg)	5	10	15
C = Sodim cholate (mg)	5	7.5	10
Dependent Variable			Goals
Y_1 = Vesicle size (nm)			<200 nm
Y_2 = PDI			<0.3
Y_3 and Y_4 = Entrapment efficiency (%)			>70%

(2 mL) was put in an Eppendorf tube and centrifuged at 10,000 rpm using a Cooling Centrifuge (C24, REMI Instruments Ltd.). The supernatant obtained was filtered (0.45 μm) after centrifugation, which was later diluted with methanol. The UV spectrophotometric evaluation of the drug concentration was conducted at wavelengths of 265.5 and 298 nm for 5-FU and SES, respectively. Assessing the drug-loading capacity of TL depends significantly on the entrapment efficiency of the drugs, a crucial determinant influenced by multiple factors such as the formulation development process, drug properties, and formulation variables.[74]

The following equations were utilized to quantify % EE and % drug loading.

$$\%\ \text{entrapment efficiency} = \frac{\text{total amount of drug} - \text{amount of free drug}}{\text{total amount of drug}} \times 100$$

$$\%\ \text{drug loading} = \frac{\text{total amount of drug entrapped}}{\text{total amount of drug and lipid}} \times 100$$

4.5.3. Morphological Studies. 4.5.3.1. Transmission Electron Microscopy. The morphology analysis of the FS-TL was examined using a transmission electron microscope (TEM; JEOL, Japan). A minute quantity of the diluted nanoformulation was deposited onto a carbon−copper grid and subsequently desiccated. Subsequently, the desiccated specimen was subjected to a solution containing phosphotungstic acid at a concentration of 1% weight/volume [34]. The specimen was subjected to further analysis using a transmission electron microscope at 70 kV.

4.5.3.2. Scanning Electron Microscopy. Before scanning electron microscopy (SEM) analysis, the aqueous FS-TL formulation underwent lyophilization to achieve a dry powdered formulation. Before freeze-drying, a cryoprotectant, specifically 5% mannitol, was incorporated into the formula-

Table 5. Stability Studies of FS-TL Formulation

Storage Time (Months)	Temperature and Humidity	Appearance	Phase separation	Vesicle size (nm)	PDI	Zeta potential (mV)
0	4 ± 0.5 °C/60 ± 5%RH	Clear	No phase separation	164.6 ± 0.5	0.269 ± 0.01	−33.17 ± 0.9
	40 ± 275 ± 5%RH	Clear	No phase separation	166.7 ± 0.2	0.275 ± 0.02	−32.04 ± 0.3
1	4 ± 0.5 °C/ °C/60 ± 5%RH	Clear	No phase separation	165.84 ± 0.9	0.274 ± 0.02	−32.82 ± 0.7
	40 ± 2 °C/75 ± 5%RH	Clear	No phase separation	171.68 ± 0.7	0.296 ± 0.03	−31.42 ± 0.5
3	4 ± 0.5 °C/60 ± 5%RH	Clear	No phase separation	166.97 ± 0.6	0.288 ± 0.01	31.90 ± 0.5
	40 ± 2 °C/75 ± 5%RH	Clear	No phase separation	175.99 ± 0.5	0.332 ± 0.05	−30.11 ± 0.6
4	4 ± 0.5 °C/60 ± 5%RH	Clear	No phase separation	167.19 ± 0.7	0.301 ± 0.01	−31.08 ± 0.8
	40 ± 2 °C/75 ± 5%RH	Cloudy	No Phase separation	198.24 ± 0.4	0.413 ± 0.03	28.28 ± 0.8
6	4 ± 0.5 °C/60 ± 5%RH	Clear	No phase separation	169.42 ± 0.6	0.302 ± 0.02	−31.05 ± 0.4
	40 ± 2 °C/75 ± 5%RH	Cloudy	Phase separation	247.51 ± 0.8	0.496 ± 0.08	−25.45 ± 0.5

https://doi.org/10.1021/acsomega.4c09147
ACS Omega 2025, 10, 6857−6875

tion.[75] SEM analysis was conducted on the lyophilized FS-TL formulation. The SEM images were received via a Hitachi S-520 electron microscope, which was operated at an accelerated voltage showing 10 kV. The samples were later mounted on aluminum stubs with the help of a double-sided adhesive tape and then subjected to gold coating in the Hitachi HUS-5 GB vacuum evaporator.[76]

4.6. Compatibility Studies. The samples of 5-FU and SES drugs were accurately weighed in a container, blended to form physical mixes, evenly crushed using a mortar and pestle, and subsequently placed into sealed glass containers resistant to light. Using DSC, XRD, and FTIR, the produced samples were analyzed.

4.6.1. FTIR. A 1−2 mg of test samples of 5-FU, SES, and FS-TL were prepared by adding the samples into a KBr and subsequently mixing and grinding them until a uniform mixture was obtained. The drug and KBr mixture were subsequently compressed into individual pellets. To obtain the infrared spectra, the pellets were subjected to analysis with the help of an FT/IR-4100 Spectrometer (Bruker Tensor 37, Massachusetts, USA) within an IR spectral range of 400−4000 cm^{-1}. Late, the obtained spectra were compared to the standard spectra of 5-FU and SES.[77]

4.6.2. DSC. The determination of the drug's physical state was obtained using a DSC (PerkinElmer Pyres, Massachusetts, USA). The pure drug sample, mixture, mannitol, and formulation DSC were performed. The liquid formulation was lyophilized, resulting in the formation of a lyophilized powder. A sample weight of 2.0 mg was later carefully placed into a standard aluminum pan. The samples were subjected to heating from 20 to 400 °C at a constant rate of 10 °C per minute. During the heating procedure, a steady stream of nitrogen gas at a flow rate of 20 mL per minute was upheld to confirm a consistent purging of the system.[78]

4.6.3. Powder X-ray Diffraction (PXRD) Analysis. The STADI P equipment provided by STOE (STOE & Cie GmbH, Darmstadt Germany) was used for the X-ray powder diffraction (XRD) investigation. This analysis aimed to examine the impact of drug-excipient mixtures, both binary and multicombination, on the crystallinity of the drugs.[79] The experimental arrangement includes a radiation source emitting Cu−Kα radiation, and a linear position-sensitive detector (PSD) serving as the detector. Measurements of pure drugs, mixture and lyophilized formulation were conducted in transmission mode with a step size of 0.15°, with every step lasting 180 s. The measurements were conducted with a voltage and current of about 40 kV and 30 mA, respectively. The range of 2θ angles used in the measurements was from 5° to 60°.[80]

4.7. Antioxidant Activity and IC_{50}. The evaluation of the DPPH radical scavenging properties of both drugs and FS-TL was carried out followed by the procedure detailed by Brand-Williams and colleagues,[81] with certain modifications. Three test samples included ascorbic acid (AA) as a standard antioxidant, 5-FU, SES, and FS-TL. A DPPH solution (0.1 mM) was prepared in methanol, and 100 μL of this solution was added to 100 μL of this solution was added to 100 μL of the test samples in a 96-well microtiter plate. Control wells were established by adding 200 μL of DPPH solution (96 μM in HPLC-grade methanol) to one group and 200 μL of methanol to another. Test samples were prepared at varying concentrations (50−300 μg/mL), with methanol serving as the blank.

The prepared samples were allowed to be placed in a dark environment and were kept at a temperature of 27 °C for 30 min, allowing them to incubate. After the incubation period, absorbance measurements were taken at 517 nm using a microplate reader (SpectraMax M2, Molecular Devices Inc., USA) connected to a computer running SoftMax Pro version 6.5.1 software for data collection and analysis.[82] The scavenging activity of the DPPH radical by each sample was calculated using the formula

$$\%\ \text{scavenging} = \frac{\text{absorbance (control)} - \text{absorbance (sample)}}{\text{absorbance (control)}} \times 100$$

The IC_{50} value, defined as the concentration required to inhibit 50% of the DPPH radicals, was determined for all test samples, including the standard AA, 5-FU, SES, and FS-TL.[83]

4.8. Combination Index (CI) Assessment. Combining two drugs may not always exceed the cumulative efficacy of administering the agents alone. The quantitative combination index (CI) values lower than 1, equal to 1, and more than 1 signify synergism, additive, and antagonistic effects, respectively. The mathematical equation below representing the calculation of the combination index (CI) is as follows:

$$\text{combination index} = \frac{dX}{DX} + \frac{dY}{DY}$$

The variables dX and dY depict IC_{50} values of drug a and drug b, respectively, when administered individually. On the other hand, the variables DX and DY highlight the IC_{50} values of drug a and drug b when administered in combined therapies.[84]

4.9. Drug Release and Kinetics Model. In a controlled laboratory environment, the drug release from the FS-TL and FS-suspension was compared using the dialysis bag technique. After adding 2 mL of TL formulation and suspension, the preactivated dialysis bags (MW: 12,000−14,000) were tightly sealed. Subsequently, the immersion of the dialysis bag was done in a 100 mL solution of dissolving media composed of phosphate buffer and methanol in a ratio of 9:1 v/v, with a pH of 5.5. The solution was equilibrated at 37 ± 2 °C and stirred at 400 rpm. A 2 mL aliquot was taken out from the beaker at specific time intervals and replaced with an equal volume of a new dissolving media. The samples were diluted with methanol and filtered (0.22 μm).[85] The quantification of the released 5-FU and SES was estimated using a UV spectrophotometer at a wavelength of 265.5 and 295 nm respectively.[86] Higuchi diffusion model, zero and first-order kinetics, and Korsmeyer-Peppas model were employed to analyze the drug release process.

4.10. Skin Permeation Study. Before conducting the skin permeation study, the developed formulation underwent conversion into a Carbopol 940P-based gel to simulate its intended application method and evaluate its performance in a representative formulation. Carbopol 934P served as the developing agent (gelling-based). It was then dissolved in water (double distilled). Subsequently, the mixture was then left undisturbed overnight to guarantee comprehensive solidification and expansion. Then, FS-TL was added to the Carbopol mixture while maintaining continuous stirring. Additionally, PEG 400 at a concentration of 5% was introduced as a humectant and plasticizer, while triethanolamine at a concentration of 0.5% was added and homogenized

https://doi.org/10.1021/acsomega.4c09147
ACS Omega 2025, 10, 6857−6875

for neutralization purposes. As a result, a transparent FS-TL gel (FS-TLG) was obtained.

In this investigation, the skin of mice was obtained following euthanasia via the technique known as cervical dislocation. The animal experimentation conducted at Jamia Hamdard was permitted by the Institutional Animal Ethics Committee (IAEC) (Protocol No. 2052, 2023). The experimental setup involved the use of Franz diffusion cells, which had a surface area of 0.785 cm^2 and were employed to investigate skin permeation in mice. Ten mL of PBS (pH 5.5) was added to the receptor compartment. It was kept at a stirring speed of 600 rpm with the help of a magnetic stirrer. The FS-TLG was administered onto the skin in the donor cell topically. The receptor cell was maintained at 37 ± 1 °C during the entire experiment, and agitation was accomplished using a magnetic bead spinning at 600 rpm. A 2 mL aliquot was taken out from the beaker at specific time points and replaced with an equal volume of a new dissolving media. The collected samples were subjected to further filtration. Later, these were then diluted with PBS 5.5. Drug concentration present in samples was measured with the help of UV spectrophotometry having a PBS 5.5 acting as a standard solution.[87]

4.11. Dermatokinetic Study. The procedures outlined in the processing of *ex vivo* skin permeation investigation were followed in the dermatokinetic experiment. Alternatively, throughout this investigation, whole skin from the Franz cell was excised at predetermined sampling time points of 0, 1, 4, 6, and 8 h. The skin samples underwent washing with a normal saline solution to eliminate any leftover formulation adhered to the skin. Following this, the sample of skin was immersed in water that was heated at 60 °C for a duration of two to three minutes. Then, using forceps with sharp, fine tips, the layers of the dermis and epidermis were diligently separated. To enhance the drug extraction process, the layers were separately fragmented into small pieces, which were immersed in a solution containing methanol for about 24 h. The methanolic solution was filtered (0.45 μm) before determining the concentration of 5-FU and SES spectrophotometrically at wavelengths of 265.5 and 295 nm, respectively. For the dermis and epidermis, the concentration of 5-FU and SES per square centimeter of skin over time was shown individually. The parameters for dermatokinetics like $T_{skin\ max}$, $C_{skin\ max}$, Ke, and AUC_{0-8h} were calculated using the p*K* Solver 3.0 program.[47]

4.12. Skin Interaction Study. The study examined the interaction between FS-TLG and skin using a differential scanning calorimeter (DSC). Two Franz diffusion cells were utilized with each cell having a phosphate buffer at a pH of 5.5 in the receptor compartment. Freshly prepared mice skins were attached to the cells. The FS-TLG was put on the skin sample attached to a Franz cell, and an 8-h permeation investigation was conducted. Within the procedure section, you could include a line. A control group consisting of untreated skin samples were kept in the donor section of a Franz diffusion cell, alongside some treated samples, to facilitate a comparative analysis of skin permeation behavior under identical experimental conditions. The skin samples were taken out of the Franz cell, properly cleaned using distilled water, and then dried when the permeation examination was completed. Afterward, the dehydrated skin sample was divided into small pieces and securely enclosed in aluminum pans for subsequent analysis using DSC.[88]

4.13. Evaluation of the Penetration Depth. Confocal laser scanning microscopy (CLSM) (410 Zeiss, Germany) was employed to evaluate the extent to which the TL gel and hydroalcoholic solution penetrated the skin. To treat the mice's skin on the Franz diffusion cell, a hydroalcoholic solution and a formulation including a mixture of Rhodamine B dye were smeared. The skin was taken off after eight hours, and any residual formulation that had adhered to it was cleaned with ethanol. Subsequently, the sample was vertically sectioned into slices with a thickness of 52 μm. These slices were then affixed onto slides, allowing for the observation of fluorescence intensity across various layers of the skin via confocal laser scanning microscopy (CLSM). Utilization of an argon laser beam at 488 and 532 nm was employed for optically exciting and detecting fluorescence emission, respectively.[89]

4.14. Skin Irritation Study. An experiment assessing skin irritation was conducted on mice's skin. A comparative investigation evaluated the potential irritation caused by the formulated product (FS-TLG) compared to a 0.8% v/v Formalin solution as a positive control whereas, no treatment as a negative control. The potential of the formulation to induce skin irritation was evaluated using the Draize test. Hair remover was used to remove hair from the mice's dorsal surface. After 24 h of administering, the formulation including treatment as well as the positive control, all the animals were regularly monitored for the presence of any erythema and edema. Severity scores that range from 0 to 4 were subsequently given based on the observed symptoms.[90]

4.15. Cytotoxicity Studies on A431 Cell Lines. The cytotoxicity of normal A431 cells was assessed with the help of (3-(4,5-dimethylthiazol-2-yl)-2,5-diphenyltetrazolium bromide (MTT) evaluation to evaluate the effects of the FS-TL and FS-suspension.[38] For this, 200 μL of A431 cell suspension containing 2×10^5 cells were seeded into each well of a 96-well plate, with three wells per condition. The plates were then incubated for 24 h at 37 °C in an atmosphere containing 5% CO_2. Following a 24-h incubation period, cells were clinged to well and exposed to different concentrations (ranging from 25 to 300 μM) of FS-TL and FS-suspension in fresh media. The cells were then incubated for a further 24 h at 37 °C. After the drug treatment, the media in each well was removed, and 10 μL of MTT solution having a concentration of 5 mg/mL in PBS was later applied to the cells. The well's capacity was augmented to 100 μL including an additional 90 μL containing fresh medium. The cells treated with MTT were placed in a 5% CO_2 atmosphere and incubated at 37 °C for 4 h. After the incubation period, the liquid culture was removed, and all the cells were subjected to washing using PBS. Following a 4-h incubation period, formazan crystals formed due to the reduction of MTT within the mitochondria. The formazan crystals were dissolved in DMSO (150 μL/well) and their presence was assessed by measuring the absorbance at 550 nm with the help of Biorad USA microplate reader.[91] The equation below is used to calculate the % cell cytotoxicity.

$$\%\ \text{cell cytotoxicity} = \frac{\text{absorbance of control} - \text{absorbance of test sample}}{\text{absorbance of control}} \times 100$$

The absorbance of control represents a measurement from untreated cells (100% viability).

4.16. Stability Studies. To evaluate the stability of the FS-TL samples, they were stored in storage conditions of 4 ± 0.5

https://doi.org/10.1021/acsomega.4c09147
ACS Omega 2025, 10, 6857−6875

°C/60 ± 5% RH and 40 ± 2 °C/75 ± 5% RH for 6 months, in accordance with ICH guidelines (Q1A R2). The evaluation parameters considered for assessment were appearance, phase separation, size of vesicle, PDI, and zeta potential.

4.17. Statistical Analysis. The experimental data underwent statistical analysis by a one-way analysis of variance (ANOVA) utilizing GraphPad Prism (v 8.0, GraphPad Software Inc., San Diego, CA, USA). Statistical significance was determined for p-values less than 0.05 and 0.0001. The reported values are expressed as the mean ± standard deviation.

■ ASSOCIATED CONTENT

Data Availability Statement

Data are contained within the article.

■ AUTHOR INFORMATION

Corresponding Authors

Asgar Ali − *Jamia Hamdard University, Department of Pharmaceutics, School of Pharmaceutical Education and Research, New Delhi, India 110062*; Phone: +91-9899571726; Email: alipharm786@gmail.com

Mohd. Aqil − *Jamia Hamdard University, Department of Pharmaceutics, School of Pharmaceutical Education and Research, New Delhi, India 110062*; Phone: +91-9811798725; Email: maqil@jamiahamdard.ac.in

Authors

Samreen Jahan − *Jamia Hamdard University, Department of Pharmaceutics, School of Pharmaceutical Education and Research, New Delhi, India 110062*

Niha Sultana − *Jamia Hamdard University, Department of Pharmaceutics, School of Pharmaceutical Education and Research, New Delhi, India 110062*

Asad Ali − *Jamia Hamdard University, Department of Pharmaceutics, School of Pharmaceutical Education and Research, New Delhi, India 110062*

Nasr A. Emad − *Jamia Hamdard University, Department of Pharmaceutics, School of Pharmaceutical Education and Research, New Delhi, India 110062*; orcid.org/0000-0003-1852-7778

Perwez Alam − *King Saud University, Department of Pharmacognosy, College of Pharmacy, Riyadh, Saudi Arabia 11451*; orcid.org/0000-0003-0668-2236

Mohd. Mujeeb − *Jamia Hamdard University, Department of Pharmacognosy and Phytochemistry, School of Pharmaceutical Education and Research, New Delhi, India 110062*

Complete contact information is available at: https://pubs.acs.org/10.1021/acsomega.4c09147

Author Contributions

Conceptualization: S.J. and Asgar Ali. Methodology: S.J., N.S., and Asad Ali. Software: S.J. and N.A.E.. Validation: N.A.E.. Formal analysis: P.A. and N.S.. Investigation: S.J. and Asgar Ali. Resources: M.A. and M.M. Data curation: Asad Ali and N.A.E.. Writing—original draft preparation: S.J.. Writing—review and editing: N.A.E., Asad Ali, P.A., and Asgar Ali. Visualization: M.A. and M.M. Supervision: Asgar Ali. Project administration: Asgar Ali. and M.A. Funding acquisition: P.A. All authors have read and agreed to the published version of the manuscript.

Funding

This research received no external funding.

Notes

All animal experiments adhered to the ARRIVE guidelines and were carried out in strict accordance with the National Research Council's Guide for the Care and Use of Laboratory Animals. Animal studies conducted at Jamia Hamdard received ethical approval from the Institutional Animal Ethics Committee (IAEC) under Protocol No. 2052, year 2023. The mentioned committee has been registered with the Committee for Control and Supervision of Experiments on Animals (CPCSEA), under registration number 173/GO/ReBi/S/2000/CCSEA.

The authors declare no competing financial interest.

■ ACKNOWLEDGMENTS

The authors acknowledge the support of the Department of Science and Technology (DST), Govt. of India for PURSE (No. SR/PURSE Phase 2/39 [C]) and FIST (No. SR/FST/LS-I/2017/85[C]) grants awarded to Jamia Hamdard and Dept. of Pharmaceutics, School of Pharmaceutical Education and Research, Jamia Hamdard. P.A. is thankful to the Researchers Supporting Project Number (RSPD2025R945), King Saud University, Riyadh, Saudi Arabia.

■ ABBREVIATIONS

5-FU 5-fluorouracil
SES sesamol
TL transliposome
FS-TL 5-fluorouracil- and sesamol-loaded transliposomes
FS-TLG 5-fluorouracil- and sesamol- loaded transliposomal gel
QbD quality by design
QTPP quality target product profile
CQAs critical quality attributes
BBD box Behnken design
PDI polydispersity index
EE entrapment efficiency
DL drug loading
TEM transmission electron microscopy
SEM scanning electron microscopy
CLSM confocal laser microscopy scanning
IC_{50} half-maximal inhibitory concentration
EPR enhanced permeability retention
FTIR Fourier transform infrared
DSC differential scanning calorimetry
XRD X-ray diffraction
AA ascorbic acid
CI combination index

■ REFERENCES

(1) Apalla, Z.; Lallas, A.; Sotiriou, E.; Lazaridou, E.; Ioannides, D. Epidemiological Trends in Skin Cancer. *Dermatol. Pract. Concept.* **2017**, *7* (2), 1−6.

(2) Afaq, F. Natural Agents: Cellular and Molecular Mechanisms of Photoprotection. *Arch. Biochem. Biophys.* **2011**, *508* (2), 144−151.

(3) Cohen, J. L. Actinic Keratosis Treatment as a Key Component of Preventive Strategies for Nonmelanoma Skin Cancer. *Journal of Clinical and Aesthetic Dermatology* **2010**, 39−44.

(4) *Melanoma Skin Cancer Statistics | American Cancer Society*. https://www.cancer.org/cancer/types/melanoma-skin-cancer/about/key-statistics.html (accessed 2024-01-18).

https://doi.org/10.1021/acsomega.4c09147
ACS Omega 2025, 10, 6857−6875

(5) Ferlay, J.; Colombet, M.; Soerjomataram, I.; Mathers, C.; Parkin, D. M.; Piñeros, M.; Znaor, A.; Bray, F. Estimating the Global Cancer Incidence and Mortality in 2018: GLOBOCAN Sources and Methods. *International Journal of Cancer.* **2019**, *144*, 1941−1953.
(6) Mangione, C. M.; Barry, M. J.; Nicholson, W. K.; Chelmow, D.; Coker, T. R.; Davis, E. M.; Donahue, K. E.; Jaén, C. R.; Kubik, M.; Li, L.; Ogedegbe, G.; Rao, G.; Ruiz, J. M.; Stevermer, J.; Tsevat, J.; Underwood, S. M.; Wong, J. B. Screening for Skin Cancer: US Preventive Services Task Force Recommendation Statement. *JAMA* **2023**, *329* (15), 1290−1295.
(7) Sohrabi, M.; Babaei, Z.; Haghpanah, V.; Larijani, B.; Abbasi, A.; Mahdavi, M. Recent Advances in Gene Therapy-Based Cancer Monotherapy and Synergistic Bimodal Therapy Using Upconversion Nanoparticles: Structural and Biological Aspects. *Biomedicine and Pharmacotherapy.* **2022**, *156*, 113872.
(8) Yap, T. A.; Omlin, A.; De Bono, J. S. Development of Therapeutic Combinations Targeting Major Cancer Signaling Pathways. *J. Clin. Oncol.* **2013**, *31* (12), 1592.
(9) Mokhtari, R. B.; Homayouni, T. S.; Baluch, N.; Morgatskaya, E.; Kumar, S.; Das, B.; Yeger, H. Combination Therapy in Combating Cancer. *Oncotarget.* **2017**, *8*, 38022−38043.
(10) Rajkumar, J.; Radha, G. V. Topical Drug Delivery of 5-Fluorouracil Proniosomal Gel for the Treatment of Skin Cancer: In Vitro and in Vivo Evaluation. *Pharm. Sci. Asia* **2021**, *48* (2), 147.
(11) Iqubal, M. K.; Iqubal, A.; Imtiyaz, K.; Rizvi, M. M. A.; Gupta, M. M.; Ali, J.; Baboota, S. Combinatorial Lipid-Nanosystem for Dermal Delivery of 5-Fluorouracil and Resveratrol against Skin Cancer: Delineation of Improved Dermatokinetics and Epidermal Drug Deposition Enhancement Analysis. *Eur. J. Pharm. Biopharm.* **2021**, *163*, 223−239.
(12) Johnston, P. G.; Kaye, S. Capecitabine: A Novel Agent for the Treatment of Solid Tumors. *Anticancer. Drugs* **2001**, *12* (8), 639−646.
(13) Ghafouri-Fard, S.; Abak, A.; Tondro Anamag, F.; Shoorei, H.; Fattahi, F.; Javadinia, S. A.; Basiri, A.; Taheri, M. 5-Fluorouracil: A Narrative Review on the Role of Regulatory Mechanisms in Driving Resistance to This Chemotherapeutic Agent. *Frontiers in Oncology.* **2021**, DOI: 10.3389/fonc.2021.658636.
(14) Longley, D. B.; Harkin, D. P.; Johnston, P. G. 5-Fluorouracil: Mechanisms of Action and Clinical Strategies. *Nat. Rev. Cancer* **2003**, *3* (5), 330−338.
(15) Fan, C.; Chen, J.; Wang, Y.; Wong, Y. S.; Zhang, Y.; Zheng, W.; Cao, W.; Chen, T. Selenocystine Potentiates Cancer Cell Apoptosis Induced by 5-Fluorouracil by Triggering Reactive Oxygen Species-Mediated DNA Damage and Inactivation of the ERK Pathway. *Free Radic. Biol. Med.* **2013**, *65*, 305−316.
(16) Goindi, S.; Arora, P.; Kumar, N.; Puri, A. Development of Novel Ionic Liquid-Based Microemulsion Formulation for Dermal Delivery of 5-Fluorouracil. *AAPS PharmSciTech* **2014**, *15* (4), 810−821.
(17) Dai, X. L.; Voronin, A. P.; Gao, W.; Perlovich, G. L.; Lu, T. B.; Chen, J. M. Intermolecular Interactions and Permeability of 5-Fluorouracil Cocrystals with a Series of Isomeric Hydroxybenzoic Acids: A Combined Theoretical and Experimental Study. *CrystEngComm* **2019**, *21* (34), 5095−5105.
(18) Fukuda, Y.; Nagata, M.; Osawa, T.; Namiki, M. Chemical Aspects of the Antioxidative Activity of Roasted Sesame Seed Oil, and the Effect of Using the Oil for Frying. *Agric. Biol. Chem.* **1986**, *50* (4), 857−862.
(19) Khamphio, M.; Barusrux, S.; Weerapreeyakul, N. Sesamol Induces Mitochondrial Apoptosis Pathway in HCT116 Human Colon Cancer Cells via Pro-Oxidant Effect. *Life Sci.* **2016**, *158*, 46−56.
(20) Siriwarin, B.; Weerapreeyakul, N.; Tanthanuch, W.; Thumanu, K. Biomolecular Changes and DNA Targeting Effect of Sesamol in Human Lung Adenocarcinoma (SK-LU-1) Cells by FTIR Microscopy. *Asian Pac. J. Trop. Biomed.* **2018**, *8* (8), 377−386.
(21) Srisongkram, T.; Weerapreeyakul, N.; Kärkkäinen, J.; Rautio, J. Role of L-Type Amino Acid Transporter 1 (LAT1) for the Selective Cytotoxicity of Sesamol in Human Melanoma Cells. *Molecules* **2019**, *24* (21), 3869.
(22) Srisongkram, T.; Weerapreeyakul, N. Route of Intracellular Uptake and Cytotoxicity of Sesamol, Sesamin, and Sesamolin in Human Melanoma SK-MEL-2 Cells. *Biomed. Pharmacother.* **2022**, *146*, 112528.
(23) Liu, Z.; Ren, B.; Wang, Y.; Zou, C.; Qiao, Q.; Diao, Z.; Mi, Y.; Zhu, D.; Liu, X. Sesamol Induces Human Hepatocellular Carcinoma Cells Apoptosis by Impairing Mitochondrial Function and Suppressing Autophagy. *Sci. Rep.* **2017**, *7*, 45728.
(24) Nair, A. B.; Dalal, P.; Kadian, V.; Kumar, S.; Kapoor, A.; Garg, M.; Rao, R.; Aldhubiab, B.; Sreeharsha, N.; Almuqbil, R. M.; Attimarad, M.; Elsewedy, H. S.; Shinu, P. Formulation, Characterization, Anti-Inflammatory and Cytotoxicity Study of Sesamol-Laden Nanosponges. *Nanomaterials* **2022**, *12* (23), 4211.
(25) Ramachandran, S.; Rajendra Prasad, N.; Karthikeyan, S. Sesamol Inhibits UVB-Induced ROS Generation and Subsequent Oxidative Damage in Cultured Human Skin Dermal Fibroblasts. *Arch. Dermatol. Res.* **2010**, *302* (10), 733.
(26) Baek, S. H.; Lee, S. H. Sesamol Decreases Melanin Biosynthesis in Melanocyte Cells and Zebrafish: Possible Involvement of MITF via the Intracellular CAMP and P38/JNK Signalling Pathways. *Exp. Dermatol.* **2015**, *24* (10), 761.
(27) Srisongkram, T.; Bahrami, K.; Järvinen, J.; Timonen, J.; Rautio, J.; Weerapreeyakul, N. Development of Sesamol Carbamate-L-Phenylalanine Prodrug Targeting L-Type Amino Acid Transporter1 (LAT1) as a Potential Antiproliferative Agent against Melanoma. *Int. J. Mol. Sci.* **2022**, *23* (15), 8446.
(28) Majdalawieh, A. F.; Mansour, Z. R. Sesamol, a Major Lignan in Sesame Seeds (Sesamum Indicum): Anti-Cancer Properties and Mechanisms of Action. *Eur. J. Pharmacol.* **2019**, *855*, 75−89.
(29) Bhardwaj, R.; Sanyal, S.; Vaiphei, K.; Kakkar, V.; Deol, P. K.; Kaur, I. P.; Kaur, T. Sesamol Induces Apoptosis by Altering Expression of Bcl-2 and Bax Proteins and Modifies Skin Tumor Development in Balb/c Mice. *Anticancer. Agents Med. Chem.* **2017**, *17* (5), 726−733.
(30) Gupta, M. K.; Sansare, V.; Shrivastava, B.; Jadhav, S. Design, Fabrication and Characterization of Sesamol Loaded Polymeric Nanoparticles: In Vivo Hepatoprotective Potential in Wistar Rats. *Nanomedicine Res. J.* **2021**, *6* (3), 296.
(31) Puglia, C.; Lauro, M. R.; Offerta, A.; Crascì, L.; Micicchè, L.; Panico, A. M.; Bonina, F.; Puglisi, G. Nanostructured Lipid Carriers (NLC) as Vehicles for Topical Administration of Sesamol: In Vitro Percutaneous Absorption Study and Evaluation of Antioxidant Activity. *Planta Med.* **2017**, *83* (5), 398−404.
(32) Attia, M. F.; Anton, N.; Wallyn, J.; Omran, Z.; Vandamme, T. F. An Overview of Active and Passive Targeting Strategies to Improve the Nanocarriers Efficiency to Tumour Sites. *J. Pharm. Pharmacol.* **2019**, *71* (8), 1185−1198.
(33) Albratty, M. Design, Optimization, and Characterization of Althaea Officinalis-Loaded Transliposomes for the Treatment of Atopic Dermatitis: A Box Behnken Design, in Vitro, and Ex Vivo Study. *J. Biomater Sci. Polym. Ed* **2023**, *34*, 2356−2375.
(34) Alhakamy, N. A.; Aldawsari, H. M.; Ali, J.; Gupta, D. K.; Warsi, M. H.; Bilgrami, A. L.; Asfour, H. Z.; Noor, A. O.; Md, S. Brucine-Loaded Transliposomes Nanogel for Topical Delivery in Skin Cancer: Statistical Optimization, in Vitro and Dermatokinetic Evaluation. *3 Biotech* **2021**, *11* (6), 288.
(35) Pereira, M. N.; Nogueira, L. L.; Cunha-Filho, M.; Gratieri, T.; Gelfuso, G. M. Methodologies to Evaluate the Hair Follicle-Targeted Drug Delivery Provided by Nanoparticles. *Pharmaceutics.* **2023**, *15*, 2002.
(36) Danaei, M.; Dehghankhold, M.; Ataei, S.; Hasanzadeh Davarani, F.; Javanmard, R.; Dokhani, A.; Khorasani, S.; Mozafari, M. R. Impact of Particle Size and Polydispersity Index on the Clinical Applications of Lipidic Nanocarrier Systems. *Pharmaceutics.* **2018**, *10*, 57.
(37) Németh, Z.; Csóka, I.; Semnani Jazani, R.; Sipos, B.; Haspel, H.; Kozma, G.; Kónya, Z.; Dobó, D. G. Quality by Design-Driven Zeta Potential Optimisation Study of Liposomes with Charge Imparting Membrane Additives. *Pharmaceutics* **2022**, *14* (9), 1798.

https://doi.org/10.1021/acsomega.4c09147
ACS Omega 2025, 10, 6857−6875

(38) Mohammed, N.; Sanoj Rejinold, N.; Mangalathillam, S.; Biswas, R.; Nair, S. V.; Jayakumar, R. Fluconazole Loaded Chitin Nanogels as a Topical Ocular Drug Delivery Agent for Corneal Fungal Infections. *J. Biomed. Nanotechnol.* **2013**, *9* (9), 1521−1531.
(39) Al-Mahallawi, A. M.; Abdelbary, A. A.; Aburahma, M. H. Investigating the Potential of Employing Bilosomes as a Novel Vesicular Carrier for Transdermal Delivery of Tenoxicam. *Int. J. Pharm.* **2015**, *485* (1−2), 329−340.
(40) Aziz, D. E.; Abdelbary, A. A.; Elassasy, A. I. Implementing Central Composite Design for Developing Transdermal Diacerein-Loaded Niosomes: Ex Vivo Permeation and In Vivo Deposition. *Curr. Drug Delivery* **2018**, *15* (9), 1330−1342.
(41) Melzak, K. A.; Melzak, S. A.; Gizeli, E.; Toca-Herrera, J. L. Cholesterol Organization in Phosphatidylcholine Liposomes: A Surface Plasmon Resonance Study. *Materials (Basel).* **2012**, *5* (11), 2306−2325.
(42) Khan, I.; Needham, R.; Yousaf, S.; Houacine, C.; Islam, Y.; Bnyan, R.; Sadozai, S. K.; Elrayess, M. A.; Elhissi, A. Impact of Phospholipids, Surfactants and Cholesterol Selection on the Performance of Transfersomes Vesicles Using Medical Nebulizers for Pulmonary Drug Delivery. *J. Drug Delivery Sci. Technol.* **2021**, *66*, 102822.
(43) Esim, O.; Bakirhan, N. K.; Sarper, M.; Savaser, A.; Ozkan, S. A.; Ozkan, Y. Influence of Emulsifiers on the Formation and in Vitro Anticancer Activity of Epirubicin Loaded PLGA Nanoparticles. *J. Drug Delivery Sci. Technol.* **2020**, *60*, 102027.
(44) Zaki, R. M.; Seshadri, V. D.; Mutayran, A. S.; Elsawaf, L. A.; Hamad, A. M.; Almurshedi, A. S.; Yusif, R. M.; Said, M. Wound Healing Efficacy of Rosuvastatin Transethosomal Gel, I Optimal Optimization, Histological and In Vivo Evaluation. *Pharmaceutics* **2022**, *14* (11), 2521.
(45) Bnyan, R.; Khan, I.; Ehtezazi, T.; Saleem, I.; Gordon, S.; O'Neill, F.; Roberts, M. Surfactant Effects on Lipid-Based Vesicles Properties. *J. Pharm. Sci.* **2018**, *107*, 1237−1246.
(46) Tabandeh, H.; Mortazavi, S. A. An Investigation into Some Effective Factors on Encapsulation Efficiency of Alpha-Tocopherol in MLVs and the Release Profile from the Corresponding Liposomal Gel. *Iran. J. Pharm. Res.* **2013**, *12*, 21−30.
(47) Alam, P.; Imran, M.; Jahan, S.; Akhtar, A.; Hasan, Z. Formulation and Characterization of Hesperidin-Loaded Transethosomal Gel for Dermal Delivery to Enhance Antibacterial Activity: Comprehension of In Vitro, Ex Vivo, and Dermatokinetic Analysis. *Gels 2023, Vol. 9, Page 791* **2023**, *9* (10), 791.
(48) Hoseini, B.; Jaafari, M. R.; Golabpour, A.; Momtazi-Borojeni, A. A.; Karimi, M.; Eslami, S. Application of Ensemble Machine Learning Approach to Assess the Factors Affecting Size and Polydispersity Index of Liposomal Nanoparticles. *Sci. Reports 2023 131* **2023**, *13* (1), 1−11.
(49) Campos, P. M.; Bentley, M. V. L. B.; Torchilin, V. P. Nanopreparations for Skin Cancer Therapy. *Nanobiomaterials in Cancer Therapy: Applications of Nanobiomaterials* **2016**, 1−28.
(50) Putri, D. C. A.; Dwiastuti, R.; Marchaban, M.; Nugroho, A. K. OPTIMIZATION OF MIXING TEMPERATURE AND SONICATION DURATION IN LIPOSOME PREPARATION. *J. Pharm. Sci. Community* **2017**, *14* (2), 79−85.
(51) Das, P.; Das, M. K. Production and Physicochemical Characterization of Nanocosmeceuticals. *Nanocosmeceuticals Innov. Appl. Saf.* **2022**, 95−138.
(52) Da Costa, S.; Basri, M.; Shamsudin, N.; Basri, H. Stability of Positively Charged Nanoemulsion Formulation Containing Steroidal Drug for Effective Transdermal Application. *J. Chem.* **2014**, *2014* (1), 748680.
(53) Cristiano, M. C.; Froiio, F.; Spaccapelo, R.; Mancuso, A.; Nisticò, S. P.; Udongo, B. P.; Fresta, M.; Paolino, D. Sulforaphane-Loaded Ultradeformable Vesicles as a Potential Natural Nanomedicine for the Treatment of Skin Cancer Diseases. *Pharmaceutics* **2020**, *12* (1), 6.
(54) Tan, F.; Li, H.; Zhang, K.; Xu, L.; Zhang, D.; Han, Y.; Han, J. Sodium Alginate/Chitosan-Coated Liposomes for Oral Delivery of Hydroxy-α-Sanshool: In Vitro and In Vivo Evaluation. *Pharmaceutics* **2023**, *15* (7), 2010.
(55) Olukman, M.; Şanlı, O.; Solak, E. K. Release of Anticancer Drug 5-Fluorouracil from Different Ionically Crosslinked Alginate Beads. *J. Biomater. Nanobiotechnol.* **2012**, *03* (04), 469−479.
(56) Gourishetti, K.; Keni, R.; Nayak, P. G.; Jitta, S. R.; Bhaskaran, N. A.; Kumar, L.; Kumar, N.; Krishnadas, N.; Shenoy, R. R. Sesamol-Loaded Plga Nanosuspension for Accelerating Wound Healing in Diabetic Foot Ulcer in Rats. *Int. J. Nanomedicine* **2020**, *15*, 9265−9282.
(57) Geetha, T.; Deol, P. K.; Kaur, I. P. Role of Sesamol-Loaded Floating Beads in Gastric Cancers: A Pharmacokinetic and Biochemical Evidence. *J. Microencapsul.* **2015**, *32* (5), 478−487.
(58) Li, P.; Yang, Z.; Wang, Y.; Peng, Z.; Li, S.; Kong, L.; Wang, Q. Microencapsulation of Coupled Folate and Chitosan Nanoparticles for Targeted Delivery of Combination Drugs to Colon. *J. Microencapsul.* **2015**, *32* (1), 40−45.
(59) Rapa, S. F.; Magliocca, G.; Pepe, G.; Amodio, G.; Autore, G.; Campiglia, P.; Marzocco, S. Protective Effect of Pomegranate on Oxidative Stress and Inflammatory Response Induced by 5-Fluorouracil in Human Keratinocytes. *Antioxidants* **2021**, *10* (2), 203.
(60) You, Y. J.; Wu, P. Y.; Liu, Y. J.; Hou, C. W.; Wu, C. S.; Wen, K. C.; Lin, C. Y.; Chiang, H. M. Sesamol Inhibited Ultraviolet Radiation-Induced Hyperpigmentation and Damage in C57BL/6 Mouse Skin. *Antioxidants* **2019**, *8* (7), 207.
(61) Miao, Z. L.; Deng, Y. J.; Du, H. Y.; Suo, X. B.; Wang, X. Y.; Wang, X.; Wang, L.; Cui, L. J.; Duan, N. Preparation of a Liposomal Delivery System and Its in Vitro Release of Rapamycin. *Exp. Ther. Med.* **2015**, *9* (3), 941−946.
(62) Fan, M.; Xu, S.; Xia, S.; Zhang, X. Preparation of Salidroside Nano-Liposomes by Ethanol Injection Method and in Vitro Release Study. *Eur. Food Res. Technol.* **2008**, *227* (1), 167−174.
(63) Gadad, A. P.; Patil, A. S.; Singh, Y.; Dandagi, P. M.; Bolmal, U. B.; Basu, A. Development and Evaluation of Flurbiprofen Loaded Transethosomes to Improve Transdermal Delivery. *Indian J. Pharm. Educ. Res.* **2020**, *54* (4), 954−962.
(64) Thakur, K.; Sharma, G.; Singh, B.; Chhibber, S.; Katare, O. P. Nano-Engineered Lipid-Polymer Hybrid Nanoparticles of Fusidic Acid: An Investigative Study on Dermatokinetics Profile and MRSA-Infected Burn Wound Model. *Drug Delivery Transl. Res.* **2019**, *9* (4), 748.
(65) Khurana, S.; Jain, N. K.; Bedi, P. M. S. Nanostructured Lipid Carriers Based Nanogel for Meloxicam Delivery: Mechanistic, in-Vivo and Stability Evaluation. *Drug Dev. Ind. Pharm.* **2015**, *41* (8), 1368−1375.
(66) Verma, D. D.; Verma, S.; Blume, G.; Fahr, A. Liposomes Increase Skin Penetration of Entrapped and Non-Entrapped Hydrophilic Substances into Human Skin: A Skin Penetration and Confocal Laser Scanning Microscopy Study. *Eur. J. Pharm. Biopharm.* **2003**, *55* (3), 271−277.
(67) Aziz, D. E.; Abdelbary, A. A.; Elassasy, A. I. Investigating Superiority of Novel Bilosomes over Niosomes in the Transdermal Delivery of Diacerein: In Vitro Characterization, Ex Vivo Permeation and in Vivo Skin Deposition Study. *J. Liposome Res.* **2019**, *29* (1), 73−85.
(68) Qadir, A.; Aqil, M.; Ali, A.; Warsi, M. H.; Mujeeb, M.; Ahmad, F. J.; Ahmad, S.; Beg, S. Nanostructured Lipidic Carriers for Dual Drug Delivery in the Management of Psoriasis: Systematic Optimization, Dermatokinetic and Preclinical Evaluation. *J. Drug Delivery Sci. Technol.* **2020**, *57*, 101775.
(69) Iqubal, M. K.; Iqubal, A.; Anjum, H.; Gupta, M. M.; Ali, J.; Baboota, S. Determination of in Vivo Virtue of Dermal Targeted Combinatorial Lipid Nanocolloidal Based Formulation of 5-Fluorouracil and Resveratrol against Skin Cancer. *Int. J. Pharm.* **2021**, *610*, 121179.
(70) Nayak, A. K.; Ahmed, S. A.; Beg, S.; Tabish, M.; Hasnain, M. S. Application of Quality by Design for the Development of Biopharmaceuticals. *Pharm. Qual. by Des. Princ. Appl.* **2019**, 399−411.

https://doi.org/10.1021/acsomega.4c09147
ACS Omega 2025, 10, 6857−6875

(71) Waghule, T.; Patil, S.; Rapalli, V. K.; Girdhar, V.; Gorantla, S.; Kumar Dubey, S.; Saha, R. N.; Singhvi, G. Improved Skin-Permeated Diclofenac-Loaded Lyotropic Liquid Crystal Nanoparticles: QbD-Driven Industrial Feasible Process and Assessment of Skin Deposition. *Liq. Cryst.* **2021**, *48* (7), 991−1009.
(72) Ahad, A.; Al-Saleh, A. A.; Al-Mohizea, A. M.; Al-Jenoobi, F. I.; Raish, M.; Yassin, A. E. B.; Alam, M. A. Formulation and Characterization of Phospholipon 90 G and Tween 80 Based Transfersomes for Transdermal Delivery of Eprosartan Mesylate. *Pharm. Dev. Technol.* **2018**, *23* (8), 787−793.
(73) Bashiri, S.; Ghanbarzadeh, B.; Ayaseh, A.; Dehghannya, J.; Ehsani, A. Preparation and Characterization of Chitosan-Coated Nanostructured Lipid Carriers (CH-NLC) Containing Cinnamon Essential Oil for Enriching Milk and Anti-Oxidant Activity. *LWT* **2020**, *119*, 108836.
(74) Ghazwani, M.; Hani, U.; Alam, A.; Alqarni, M. H. Quality-by-Design-Assisted Optimization of Carvacrol Oil-Loaded Niosomal Gel for Anti-Inflammatory Efficacy by Topical Route. *Gels 2023, Vol. 9, Page 401* **2023**, *9* (5), 401.
(75) Imam, S. S.; Ahad, A.; Aqil, M.; Akhtar, M.; Sultana, Y.; Ali, A. Formulation by Design Based Risperidone Nano Soft Lipid Vesicle as a New Strategy for Enhanced Transdermal Drug Delivery: In-Vitro Characterization, and in-Vivo Appraisal. *Mater. Sci. Eng., C* **2017**, *75*, 1198−1205.
(76) Sultana, N.; Ali, A.; Waheed, A.; Jabi, B.; Yaqub khan, M.; Mujeeb, M.; Sultana, Y.; Aqil, M. Dissolving Microneedle Transdermal Patch Loaded with Risedronate Sodium and Ursolic Acid Bipartite Nanotransfersomes to Combat Osteoporosis: Optimization, Characterization, in Vitro and Ex Vivo Assessment. *Int. J. Pharm.* **2023**, *644*, 123335.
(77) Bhatt, P.; Narvekar, P.; Lalani, R.; Chougule, M. B.; Pathak, Y.; Sutariya, V. An in Vitro Assessment of Thermo-Reversible Gel Formulation Containing Sunitinib Nanoparticles for Neovascular Age-Related Macular Degeneration. *AAPS PharmSciTech* **2019**, *20* (7), 281.
(78) Sarmento, B.; Ferreira, D.; Veiga, F.; Ribeiro, A. Characterization of Insulin-Loaded Alginate Nanoparticles Produced by Ionotropic Pre-Gelation through DSC and FTIR Studies. *Carbohydr. Polym.* **2006**, *66* (1), 1−7.
(79) Aminu, N.; Chan, S.-Y.; Mumuni, M. A.; Umar, N. M.; Tanko, N.; Zauro, S. A.; Aminu, A.; Toh, S.-M. Physicochemical Compatibility Studies of Triclosan and Flurbiprofen with Excipients of Pharmaceutical Formulation Using Binary, Ternary, and Multi-Combination Approach. *Futur. J. Pharm. Sci. 2021 71* **2021**, *7* (1), 1−16.
(80) Haider, M. S.; Schreiner, J.; Kendl, S.; Kroiss, M.; Luxenhofer, R. A Micellar Mitotane Formulation with High Drug-Loading and Solubility: Physico-Chemical Characterization and Cytotoxicity Studies in 2D and 3D In Vitro Tumor Models. *Macromol. Biosci.* **2020**, *20* (1), 1900178.
(81) Brand-Williams, W.; Cuvelier, M. E.; Berset, C. Use of a Free Radical Method to Evaluate Antioxidant Activity. *LWT - Food Science and Technology* **1995**, *28*, 25−30.
(82) Mapeka, T. M.; Sandasi, M.; Viljoen, A. M.; van Vuuren, S. F. Optimization of Antioxidant Synergy in a Polyherbal Combination by Experimental Design. *Molecules* **2022**, *27* (13), 4196.
(83) Rajesh, P.; Natvar, P. In Vitro Antioxidant Activity of Coumarin Compounds by DPPH, Super Oxide and Nitric Oxide Free Radical Scavenging Methods. *J. Adv. Pharm. Educ. Res.* **2011**, *1*, 52−68.
(84) Othman, N.; Nurul, S.; Jamil, A. M.; Mas, A.; Masarudin, J.; Ruqayyah, C.; Bashirah, A.; Jusoh, M.; Alamassi, M. N. Increased Radical Scavenging Activity of Thymoquinone and l -Ascorbic Acid Dual Encapsulated in Palmitoyl-Chitosan Nanoparticles in a Human Normal Lung Fibroblast, MRC-5 Due to Synergistic Antioxidative Effects. *RSC Adv.* **2023**, *13* (40), 27965−27983.
(85) Jahan, S.; Aqil, M.; Ahad, A.; Imam, S. S.; Waheed, A.; Qadir, A.; Ali, A. Nanostructured Lipid Carrier for Transdermal Gliclazide Delivery: Development and Optimization by Box-Behnken Design. *Inorganic and Nano-Metal Chemistry* **2022**, 474−487.
(86) Balzus, B.; Colombo, M.; Sahle, F. F.; Zoubari, G.; Staufenbiel, S.; Bodmeier, R. Comparison of Different in Vitro Release Methods Used to Investigate Nanocarriers Intended for Dermal Application. *Int. J. Pharm.* **2016**, *513* (1−2), 247−254.
(87) Aodah, A. H.; Hashmi, S.; Akhtar, N.; Ullah, Z.; Zafar, A.; Zaki, R. M.; Khan, S.; Ansari, M. J.; Jawaid, T.; Alam, A.; Ali, M. S. Formulation Development, Optimization by Box-Behnken Design, and In Vitro and Ex Vivo Characterization of Hexatriacontane-Loaded Transethosomal Gel for Antimicrobial Treatment for Skin Infections. *Gels* **2023**, *9* (4), 322.
(88) Qureshi, M.; Qadir, A.; Aqil, M.; Sultana, Y.; Warsi, M. H.; Ismail, M. V.; Talegaonkar, S. Berberine Loaded Dermal Quality by Design Adapted Chemically Engineered Lipid Nano-Constructs-Gel Formulation for the Treatment of Skin Acne. *J. Drug Delivery Sci. Technol.* **2021**, *66*, 102805.
(89) Imran, M.; Iqubal, M. K.; Imtiyaz, K.; Saleem, S.; Mittal, S.; Rizvi, M. M. A.; Ali, J.; Baboota, S. Topical Nanostructured Lipid Carrier Gel of Quercetin and Resveratrol: Formulation, Optimization, in Vitro and Ex Vivo Study for the Treatment of Skin Cancer. *Int. J. Pharm.* **2020**, *587*, 119705.
(90) Alam, M. S.; Sultana, N.; Rashid, M. A.; Alhamhoom, Y.; Ali, A.; Waheed, A.; Ansari, M. S.; Aqil, M.; Mujeeb, M. Quality by Design-Optimized Glycerosome-Enabled Nanosunscreen Gel of Rutin Hydrate. *Gels* **2023**, *9* (9), 752.
(91) Khan, M. F.; Siddiqui, S.; Zia, Q.; Ahmad, E.; Jafri, A.; Arshad, M.; Jamal, A.; Alam, M. M.; Banawas, S.; Alshehri, B. A.; Baazeem, A.; Althobaiti, F.; Ansari, A. H.; Mohammadi, A. A. Characterization and in Vitro Cytotoxic Assessment of Zinc Oxide Nano-Particles in Human Epidermoid Carcinoma Cells. *J. Environ. Chem. Eng.* **2021**, *9* (4), 105636.

https://doi.org/10.1021/acsomega.4c09147
ACS Omega 2025, 10, 6857−6875